STUDENT JOURNAL OF PHYSICS

Volume 5 **Number 4** **June 2016**

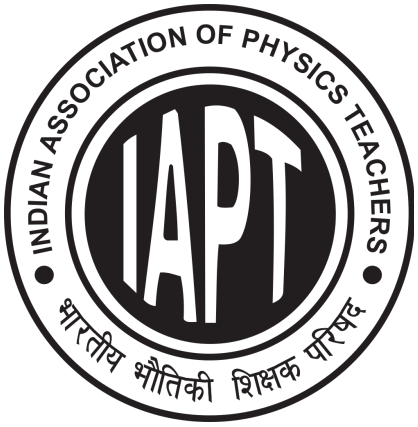

INDIAN ASSOCIATION OF PHYSICS TEACHERS

TURNING POINT

Casimir Effect-Reality Of Quantum Field Vacuum

Arvind Kumar
Homi Bhabha Centre for Science Education, Tata Institute of Fundamental Research, Mumbai 400005

Abstract. The vacuum of a quantized field manifests itself physically (Casimir Effect) when it is altered by changing the boundary conditions of the field. A well-known example of Casimir effect is the attractive force between two neutral parallel conducting plates. In this article we give a brief introduction to this topic that should be accessible to senior undergraduates. We confine our discussion to the case of a massless scalar field in two-dimensional space-time to illustrate the usual field theoretic techniques to calculate the Casimir force explicitly.

Communicated by: D.P. Roy

1. INTRODUCTION

Among the distinctive aspects of quantum mechanics is the notion of zero-point energy–the energy of the ground state of a quantum system. Classically, the lowest energy of a system is zero, if we take the zero of its potential energy at its minimum. For example, a classical oscillator in its ground state is at rest (zero kinetic energy) at its equilibrium position (where potential energy is minimum–zero by choice). Not so with a quantum oscillator which even in its ground state must have non-zero total energy. The Uncertainty Principle disallows the quantum oscillator to be simultaneously at rest (p=0) and at its mean position (x=0) exactly. The Uncertainty product $\Delta x \Delta p$ for a linear harmonic oscillator in its ground state is $\hbar/2$ and its ground state energy is $\hbar\omega/2$, where ω is the angular frequency of the oscillator. An assembly of such oscillators in thermodynamic equilibrium has some zero-point energy even at absolute zero temperature.

The proof of this result ($E_0 = \hbar\omega/2$) for a linear oscillator appears in every textbook on quantum mechanics [1]. Yet it is worth summarizing both because of its elegance and the fact that analogous features arise in field theory also, as we see in sec.2. The Hamiltonian H of a linear oscillator is:

$$H = \frac{p^2}{2m} + \frac{kx^2}{2}; \qquad k = m\omega^2 \tag{1}$$

with the usual meanings for the symbols. Define the dimensionless operators:

$$a = \frac{i(p - im\omega x)}{\sqrt{(2m\hbar w)}}, \qquad a^\dagger = -\frac{i(p + im\omega x)}{\sqrt{(2m\hbar w)}} \tag{2}$$

These operators have some remarkable properties: (i)The fundamental commutator $[x, p] = i\hbar$ translates to

$$[a, a^\dagger] = 1 \tag{3}$$

(ii)H can be rewritten in terms of a and $a^\dagger$ as:

$$H = \hbar\omega(a^\dagger a + 1/2) \tag{4}$$

(iii)The operator$a(a^\dagger)$ acting on an energy eigenstate lowers (raises) the energy of the state by $\hbar\omega$ In view of (iii),the ground state denoted by $|0\rangle$ satisfies $a|0\rangle = 0$. Then using eq. (4), $H|0\rangle = \frac{1}{2}\hbar\omega|0\rangle$,that is the ground state energy is $\frac{1}{2}\hbar\omega$.

What can we say analogously about the ground state energy of a quantum field? We take this up in detail in sec.2, but to anticipate, a classical field can be viewed as a Fourier sum of its modes; recall, a mode of a classical system is an oscillatory motion with a characteristic frequency. Applying the usual (canonical) quantization methods, the Hamiltonian of the field is found to be

$$H = \sum_{\bar{k}} (a^\dagger_{\bar{k}} a_{\bar{k}} + 1/2)\hbar\omega_{\bar{k}} \tag{5}$$

where

$$[a_{\bar{k}}, a^\dagger_{\bar{k}'}] = \delta_{\bar{k}\bar{k}'} \tag{6}$$

and all other commutators vanish.

The summation is over all the modes, regarded discrete for convenience here. The mathematics now is evidently similar to the single particle case described earlier. Accordingly, the ground state, the vacuum, of the field has energy

$$E_0 = 1/2 \sum_{\bar{k}} \hbar\omega_{\bar{k}} \tag{7}$$

which is just the earlier result summed over all the modes. Thus, whereas a classical field vacuum has zero energy, a quantized field even in its vacuum state has energy arising due to fluctuations of the field. The field averages out to zero in the vacuum state, but the the energy (a quadratic function in field) is non-zero, given by eq. (7). This is the zero-point energy of a quantum field.

But there is a problem. The sum in eq.(7) is divergent: the energy of the vacuum is infinite! This is the first of the many infinities that quantum field theory encounters [2]. However, the particular infinity encountered above is usually regarded inconsequential. The argument goes that what is observable is the difference in energy between the different energy states of the field and this energy difference is finite, as desired. It does not matter if the the absolute value of vacuum energy is infinite–it is unobservable anyway.

More than sixty years ago, an insight due to Casimir added a new twist to this argument [3]. If the vacuum energy itself is unobservable, may be a change in vacuum energy is observable. How

to bring about this change? The simplest way is to introduce (macroscopic) surfaces in space where the fields satisfy some boundary conditions (e.g. they vanish at the surfaces.) The altered boundary conditions change the possible modes of the field. The sum over modes analogous to that in eq.(7) continues to be infinite, but the new infinity is different from the earlier infinity. Their difference is finite and depends on the geometrical parameters of the configuration and the nature of boundary conditions. For example, if you introduce two parallel neutral conducting planes in space a distance a apart, the difference in the energy of the two vacuas can be shown to go like $1/a^3$. Consequently, the force between them (negative derivative of energy difference with respect to a) goes like $1/a^4$. This force can be (and has been) experimentally measured. This observation demonstrating the physical reality of the quantized field vacuum is known as Casimir Effect.

2. CASIMIR EFFECT: THE SCALAR FIELD

To illustrate the technique of calculating the Casimir force, we consider in some detail the simplest case–that of a massless scalar field in two dimensions (one space-one time). Our entire treatment in this article follows ref.[4]. The Klein Gordon equation for $m = 0$ case is the usual wave equation:

$$\Box\phi \equiv \frac{1}{c^2}\frac{\partial^2\phi(x,t)}{\partial t^2} - \frac{\partial^2\phi(x,t)}{\partial x^2} = 0 \tag{8}$$

The conserved current associated with eq.(8) is:

$$j_\mu = \phi_2^\star \frac{\partial\phi_1}{\partial x^\mu} - \frac{\partial\phi_2^\star}{\partial x^\mu}\phi_1 \tag{9}$$

$x^\mu : (x^0 = ct, x)$

$$\frac{\partial j_\mu}{\partial x_\mu} = 0 \tag{10}$$

The integral of the time component of the 4-current gives a definition of the inner product of any two solutions of the wave equation:

$$(\phi_2, \phi_1) = i\int dx \quad (\phi_2^\star \frac{\partial\phi_1}{\partial x^0} - \frac{\partial\phi_2^\star}{\partial x^0}\phi_1) \tag{11}$$

Note that eq.(11) implies indefinite norm; that is,the norm (ϕ, ϕ) is not positive definite.[This is unlike the Schrodinger and Dirac equations which give positive definite norm.] This is one reason the equation cannot be interpreted as a single particle equation. But it is fine as a field equation,which on quantization, describes spin zero particles.

Consider first the free field unbounded case,that is, when no boundary conditions are imposed. A complete orthonormal set of solutions in this case is:

$$\phi_k^\pm(x,t) = (\frac{c}{4\pi\omega})^{1/2} e^{\pm i(kx-\omega t)}; \qquad \omega = c|k|, \quad k : (-\infty, \infty) \tag{12}$$

where $\phi^+(x,t)(\phi^-(x,t))$ represent positive (negative) energy solutions. They are easily seen to be orthogonal with respect to the inner product defined already,eq.(11). The over-all constant ensures they are normalized:

$$(\phi_k^{\pm}(x,t), \phi_{k'}^{\pm}(x,t)) = \pm\delta(k-k'); \quad (\phi_k^{\pm}(x,t), \phi_{k'}^{\mp}(x,t)) = 0 \tag{13}$$

We expand the field $\phi(x,t)$ using this orthonormal set:

$$\phi(x,t) = \int_{-\infty}^{+\infty} dk \quad (a(k)\phi_k^+(x,t) + a^\dagger(k)\phi_k^-(x,t)) \tag{14}$$

Canonical quantization of the field consists in postulating the commutation relations:

$$[a(k), a^\dagger(k'] = \delta(k-k'), \tag{15}$$

with all other commutators being zero.

These lead to the expected equal time commutation relations:

$$[\phi(x,t), \dot{\phi}(x',t)] \quad = \quad ic\,\delta(x-x') \tag{16}$$

where the dot denotes differentiation with respect to time. The vacuum is defined by

$$a(k)|0\rangle = 0, \tag{17}$$

for all k. The energy density of the field is the zero-zero component of the energy momentum tensor $T_{\mu\nu}(x,t)$ of the field. It is given by

$$T_{00}(x,t) = \frac{\hbar c}{2}[\frac{1}{c^2}(\frac{\partial\phi}{\partial t})^2 + (\frac{\partial\phi}{\partial x})^2] \tag{18}$$

This is the same as the Hamiltonian density $\mathcal{H}$ of the scalar field obtained as usual from the Lagrangian density:

$$\mathcal{L} = \frac{\hbar c}{2}[\frac{1}{c^2}(\frac{\partial\phi}{\partial t})^2 - (\frac{\partial\phi}{\partial x})^2] \tag{19}$$

with

$$\mathcal{H} = \pi\dot{\phi} - \mathcal{L}, \pi \equiv \frac{\partial\mathcal{L}}{\partial\dot{\phi}} \tag{20}$$

The vacuum energy density is then obtained by taking the expectation value of T_{00} in the vacuum state. Using eqs.(14),(15)and (17), this gives after a few steps:

$$\langle 0|T_{00}|0\rangle = \frac{\hbar}{2\pi}\int_0^\infty \omega\, dk, \qquad \omega = c|k| \tag{21}$$

The total vacuum energy is the integral of eq.(21) over the entire x-axis. For later comparison, we integrate it over the interval $(0,a)$ to get

$$E_0(a) = \frac{\hbar a}{2\pi}\int_0^\infty \omega\, dk, \qquad \omega = c|k| \tag{22}$$

This is, of course, infinite, as was mentioned in sec.1.

Next, we consider the scalar field over the interval $(0, a)$ with the following boundary conditions:

$$\phi(0,t) = \phi(a,t) = 0 \tag{23}$$

This is the one-dimensional analogue of the realistic 3-dimensional case of Casimir effect for electromagnetic field when two plane neutral conductors are placed parallel at a distance a apart. (See sec.3.) We need to find the new orthonormal set of modes which satisfy the boundary conditions above. This is given by

$$\phi_n^{\pm}(x,t) = (\frac{c}{a\omega_n})^{1/2} e^{\mp(i\omega_n t)} \sin k_n x \tag{24}$$

with

$$k_n = \frac{n\pi}{a}, n = 1, 2, 3, ...; \omega_n = ck_n \tag{25}$$

The property of orthonormality of this set over the interval $(0, a)$ is given by

$$(\phi_n^{\pm}, \phi_{n'}^{\pm}) = \pm\delta_{nn'} \quad ; \quad (\phi_n^{\pm}, \phi_{n'}^{\mp}) = 0 \tag{26}$$

In eq.(26), the index n is discrete, in contrast to the continuous index k in eq.(13), since the boundary conditions,eq.(23) make k (and hence ω) discrete. Accordingly, the expansion of $\phi(x,t)$ in terms of the new orthonormal set is now a sum, not an integral:

$$\phi(x,t) = \sum_{n=1}^{\infty} [(a_n \phi_n^+(x,t) + a_n^\dagger \phi_n^-(x,t)] \tag{27}$$

where $a_n, a_n^\dagger$ satisfy the discrete version of the commutation relations of eq.(15):

$$[a_n, a_{n'}^\dagger] = \delta_{nn'} \ , \quad [a_n, a_{n'}] = [a_n^\dagger, a_{n'}^\dagger] = 0 \tag{28}$$

Using eqs.(24) to (28), we get after a straightforward calculation:

$$\frac{1}{c^2}\langle 0|\dot{\phi}^2|0\rangle = \frac{1}{ac}\sum \omega_n \sin^2 k_n x; \frac{1}{c^2}\langle 0|(\frac{\partial\phi}{\partial x})^2|0\rangle = \frac{1}{ac}\sum \omega_n \cos^2 k_n x \tag{29}$$

The energy density of the new vacuum $|0\rangle_c$ is then given by

$${}_c\langle 0|T_{00}|0\rangle_c = \frac{\hbar}{2a}\sum_{n=1}^{\infty} \omega_n \tag{30}$$

The total vacuum energy over the interval $(0, a)$ is obtained by integrating eq.(30) over 0 to a. Thus the zero-point energy of the new vacuum is :

$$E_0^c(a) = \frac{\hbar}{2}\sum_{n=1}^{\infty} \omega_n \tag{31}$$

which is again infinite.

Regularization

As seen above, both the Minkowski vacuum $|0\rangle$ and the Casimir vacuum $|0\rangle_c$ have infinite zero-point energy. We need to extract out a (possibly) finite difference between these two infinities. A general technique to do this involves what is known as 'regularization'. In brief, this consists of the following steps: (i) First get rid of the infinities in eqs.(22) and (31) by modifying the divergent integral/sum say by introducing a damping parameter suitably. When the parameter is set to its 'unregularized' value, the sum/integral, of course, diverges. (ii) Take the difference between the two regularized (i.e.finite) quantities. (iii) Finally, return to the original theory by taking the parameter to its 'unregularized' value. The difference obtained in (ii) continues to remain finite. This is the 'renormalized' zero-point energy of the Casimir vacuum. Such techniques are essential in most successful quantum field theories, such as,for example quantum electrodynamics(QED). Regularization consists in rendering the infinite integrals finite. [The damping parameter technique is not the only possible way; a more common technique is to change the dimension of the integration, the so called dimensional regularization that we cannot discuss here. In any case, the final physical result should be independent of which method of regularization is used.] Renormalization consists in redefining physical parameters (e.g. charge, mass in QED or, in our simple case, the vacuum energy] in terms of their 'bare' values, the infinities of the theory being concealed in the unobservable relations between them. These techniques are mathematically quite involved for QED and other standard field theories, but for our illustrative case, the mathematics is simple.

We adopt the damping parameter technique to regularize the infinite integral in eq.(22) and the infinite sum in eq.(31). The sum in eq.(31) is modified as follows:

$$E_0^c(a,\delta) = \frac{\hbar}{2}\sum_{n=1}^{\infty}\omega_n e^{-\delta\omega_n} \tag{32}$$

The 'unregularized sum is obtained by taking the limit $\delta \to 0$. Using the expression for the modes ω_n from eq.(25),

$$E_0^c(a,\delta) = \frac{\hbar}{2}\sum_{n=1}^{\infty}\frac{c\pi n}{a}e^{-\delta\frac{c\pi n}{a}} \tag{33}$$

This can be written as

$$E_0^c(a,\delta) = -\frac{\hbar}{2}\frac{d}{d\delta}(\sum_{n=1}^{\infty}e^{-\delta\frac{c\pi n}{a}}) \tag{34}$$

The geometrical sum in the bracket on the right side of eq.(34) is easily carried out. Differentiating that with respect to δ leads to the finite (regularized) quantity:

$$E_0^c(a,\delta) = \frac{\hbar\pi c}{8a}\ sinh^{-2}(\frac{\delta c\pi}{2a}) \tag{35}$$

To isolate the part that is singular in the 'unregularized' limit ($\delta \to 0$). we obtain E_0^c for small δ:

$$E_0^c(a,\delta) = \frac{\hbar a}{2\pi c\delta^2} - \frac{\hbar\pi c}{24a} + 0(\delta^2) \tag{36}$$

It is the first term in eq.(36) that goes to infinity as we return to the original theory. A similar method is employed to regularize the integral in eq.(22) and isolate the singularity of the original theory:

$$E_0(a,\delta) = \frac{\hbar a}{2\pi}\int_0^\infty \omega e^{-\omega\delta}dk = \frac{\hbar ac}{2\pi}\int_0^\infty k e^{-c\delta k}dk = \frac{\hbar a}{2\pi c\delta^2} \tag{37}$$

The difference in the two regularized vacuum energies is:

$$E_0^c(a,\delta) - E_0(a,\delta) = -\frac{\hbar\pi c}{24a} + 0(\delta^2) \tag{38}$$

Finally, we return to the original theory by taking $\delta \to 0$. The first term in eq.(38) is independent of δ and survives, while all the remaining terms vanish. The renormalized zero-point energy of the Casimir vacuum then is:

$$E_0'^c(a) = -\frac{\hbar\pi c}{24a} \tag{39}$$

Since this decreases with decreasing a, there is an attractive force between the boundary 'surfaces'(points in this case):

$$F(a) = -\frac{\partial E_0'^c(a)}{\partial a} = -\frac{\hbar\pi c}{24a^2} \tag{40}$$

The calculation for the massive scalar field ($m \neq 0$ case) is along the same lines.The Klein-Gordon equation for the massive case is:

$$(\Box + \frac{m^2c^2}{\hbar^2})\phi(x,t) = 0 \tag{41}$$

Eqs.(9),(10) and (11) continue to hold. The orthonormal sets for the unbounded and bounded cases are again given by eqs.(12)and (24) respectively, but the expression for the mode frequencies is altered for the two cases to

$$\omega^2 = c^2k^2 + \frac{m^2c^4}{\hbar^2}, \omega_n^2 = \frac{c^2\pi^2n^2}{a^2} + \frac{m^2c^4}{\hbar^2} \tag{42}$$

The expressions for the unregularized vacuum energy in the two cases, eqs.(22) and (31), remain unaltered in terms of the mode frequencies. However, as can be expected, the relation between ω and k (or ω_n and k_n) for the massive case complicates the evaluation of the regularized sum and integral. Consequently, the renormalized Casimir vacuum energy no longer has the simple form given by eq.(39). The Casimir force is still attractive, but smaller than for the massless case [4].

3. CASIMIR FORCE BETWEEN PARALLEL CONDUCTING PLANES

Here, the vacuum energy of the electromagnetic field is altered with change in boundary conditions of the field when two conductors are introduced in space. The analysis is much along the same lines as for the massless scalar field treated in sec.2; but now we are in 4-dimensional space-time and the

boundary conditions refer to two-dimensional surfaces–two infinite parallel conducting planes at a distance a.The photon field has two independent polarizations both of which satisfy the boundary condition that they vanish at the planes (say $z = 0$ and $z = a$). The vacuum energy density of the free electromagnetic field in the unbounded case is the 3-dimensional generalization of eq.(21):

$$\langle 0|T_{00}|0\rangle = \frac{\hbar}{(2\pi)^3}\int_0^\infty d^3k\,\omega_{\bar{k}}, \qquad \omega_{\bar{k}} = c(k_x^2 + k_y^2 + k_z^2)^{1/2} \tag{43}$$

When the boundary conditions are imposed,k_z is quantized ($k_z = n\pi/a, n = 1, 2, ...$) while k_x, k_y remain continuous. The mode frequencies then are:

$$\omega_{k_x,k_y,n} = c(k_x^2 + k_y^2 + (\frac{n\pi}{a})^2)^{1/2}, n = 1, 2, ... \tag{44}$$

For the new vacuum, the energy of the electromagnetic field between the plates is given by the generalization of eq.(31);

$$E_0^c = \frac{\hbar}{(2\pi)^2}\int dk_x dk_y \sum_{n=1}^{\infty}\omega_{k_x,k_y,n} \tag{45}$$

where an extra factor of 2 in eq.(45) arises due to the two states of polarization of the field.

As before, both the integral in eq.(43) and the sum/integral in eq.(45) are divergent,and we must regularize each using say the technique of damping parameter. We then take the difference of the two regularized vacuum energies and return to the original theory by taking the parameter to its 'unregularized' value. The actual calculation is much more mathematically involved than in sec.2. We quote the final result, which is the counterpart of eq.(39):

$$E_0'^c/S = -\frac{\hbar c\pi^2}{720a^3} \tag{46}$$

where S is the surface area of the parallel plates. Eq.(46) gives the well-known result for the Casimir force between two neutral parallel conducting plates at a distance a :

$$F(a) = -\frac{\partial E_0'^c}{\partial a} = -\frac{\hbar c\pi^2}{240a^4}S \tag{47}$$

Putting the values of $\hbar$ and c, this results in Casimir stress (force per unit area) given by

$$f(a) = -\frac{1.30\times 10^{-27}}{a^4}Nm^2 \tag{48}$$

The effect is numerically rather small and requires a to be small enough (of the order of μm) so that it does not get clouded by the effect due to small departures from neutrality of the plates. If $S = 1cm^2, a = 1\mu m$, then $F = 10^{-7}N$.

The first attempt to measure Casimir force between two metal plates was made as early as 1958, using a sensitive force balance based on a spring. From the measurement of the capacitance of the two-plate system, the extension of the spring balance and hence the force was determined [5]. In recent decades, Atomic Force Microscopy and other techniques have vastly enhanced the sensitivity of Casimir force measurement. Alongside, theoretical calculations have greatly improved, correcting for factors like finite conductivity, roughness, finite temperature effects, etc. The agreement between theory and experiment has been demonstrated [4,6].

4. CONCLUSION

In this article, we have attributed Casimir force between neutral conductors to the change in quantized electromagnetic field vacuum energy with change in boundary conditions. However, Casimir force can also be viewed as a purely relativistic quantum mechanical effect. That is, we can regard it as a summation of the microscopic forces between the molecules of the two conducting plates. The dipole-dipole interaction energy is given by the well-known formula:

$$H_{int} = \frac{\bar{\mu_1}.\bar{\mu_2}r^2 - 3(\bar{\mu_1}.\bar{r})(\bar{\mu_2}.\bar{r})}{r^5} \tag{49}$$

where $\bar{\mu_1}$ and $\bar{\mu_2}$ are the two dipole moments and $\bar{r}$ is the relative co-ordinate vector. The first order perturbation effect vanishes (for randomly oriented dipoles). The second order perturbation effect clearly goes like r^{-6} [1]. Physically, this means the fluctuating electric dipole of one molecule generates an electric field that interacts with the electric dipole of the other. However, a relativistic treatment would include retardation effect and the interaction energy then goes like r^{-7}. This latter result was first proved by Casimir and Polder [7], which was later extended by Lifshitz [8] for force between dielectric macroscopic bodies. In the appropriate limit of the dielectric constant, Lifshitz's result reduces to the result obtained by Casimir [3] using the vacuum energy approach. The equivalence between these two approaches continues to be studied for other cases also.

Casimir effect depends on the configuration and nature of boundary surfaces. An important early insight was that Casimir force is not necessarily attractive. For a perfectly conducting thin spherical shell, Casimir force (force between two halves of the shell) has been shown to be repulsive. For the case of a rectangular box, its sign depends on the ratio of height to base. For a cylindrical geometry, it is again attractive.

Lastly, Casimir effect has been studied for different topological configurations in flat and curved manifolds. For example,the one–space dimensional Casimir effect involving the material boundary condition $\phi(x = 0, t) = \phi(x = a, t) = 0$ may be looked at as non-zero vacuum energy for a flat manifold with the topology of a circle S^1. Casimir effect has also been invoked for spontaneous compactification of extra spatial dimensions in higher dimensional (Kaluza-Klein) field theories. Indeed the contexts where Casimir effect is relevant are truly diverse and span many fields of physics. Readers interested in the diverse and advanced applications of the Casimir effect can look up references [4] and [6] and the references given therein.

References

[1] .See,for example, L.I Schiff:Quantum Mechanics(3rd ed.),McGraw-Hill

[2] For an elementary introduction, see, for example, F.Mandl and G. Shaw: Quantum Field Theory (2nd ed.) Wiley

[3] H.B.G. Casimir : Proc. Kon. Nederl. Akad. Wet 51 (1948) 793

[4] M. Bordag, U. Mohideen, V.M. Mostepanenko: New Developments in the Casimir Effect, Physics Reports 353 (2001) 1-205

[5] M.J.Sparnaay, Physica 24 (1958) 751
[6] K.A. Milton :The Casimir Effect (World Scientific)
[7] H.B.G.Casimir and D.Polder : Phys. Rev. 73 (1948) 360.
[8] E.M.Lifshitz, Sov.Phys. JETP 2 (1956) 73

Studies on Liquid Mixtures Using Free Length Theory

Arya S.S* **and Bindu R.G.†**
*Fourth semester M.Sc. Physics, Mahatma Gandhi College, Thiruvananthapuram - 695004, India.
†Assistant Professor in Physics, Mahatma Gandhi College, Thiruvananthapuram - 695004, India.

Abstract. The study of intermolecular free length is being increasingly used as a tool for investigating the properties of liquid mixtures and the nature of intermolecular interaction between its components. A temperature dependent relation of intermolecular free length is derived from the standard formula of Jacobson free length equation. The validity of the relation is established using the published data on methyl ethyl ketone(MEK)+methanol(ML) and methyl phenyl ketone(MPK)+methanol(ML) from the literature. The results are discussed on the basis of molecular in- teractions present in them.
Keywords: intermolecular free length, ultrasonics, methyl ethyl ketone, methyl phenyl ketone.

Communicated by: D.P. Roy

1. INTRODUCTION

One of the most remarkable observations in physical science is that most substances, with a well defined chemical composition, can exist in one of several states, exhibiting very different physical properties on the macro- scopic scale. More over one can transform the substance from one state to another, simply by varying thermodynamic conditions like temperature or pressure. The most common states are either solid or uid in character, and are characterized by qualitatively different responses to an applied stress. At ambient temperature, the solid states of matter are generally associated with the mineral world, while 'soft' matter, and in particular the liquid state, are more intimately related to life sciences. In fact it is generally accepted that life took its origin in the primordial oceans, thus underlining the importance of a full quantitative understanding of liquids.

The study of intermolecular interaction plays an important role in the development of molecular science. A large number of studies have been made on the molecular interaction of liquid systems by various physical methods like Infrared, Raman effect, Nuclear magnetic resonance, Dielectric constant, Ultra violet and Ultrasonic methods. In recent years, Ultrasonic technique has become a powerful tool in providing information regarding the molecular behavior of the medium.

The intermolecular forces responsible for the molecular interactions can be classified as long range forces and short range forces. The long range forces are the electrostatic induction and dispersion forces and they arise when the molecules come close enough together causing a significant overlap of electron clouds and are often highly directional.

The liquid mixtures show a non linear variation of ultrasonic velocity, compressibility and other related parameters with structural changes occur- ring in a liquid when its concentration and temperature are varied.

The nonlinear variation of adiabatic compressibility of a solution with concentration of the solute was qualitatively described to hydrogen bonding and their result confirms that the sign and magnitude of such deviation depends on the strength of interaction between unlike molecules.

Though spectroscopic methods play a major role in the molecular in- teraction studies, the non-spectral studies such as calorimetric, magnetic, ultrasonic velocity and viscosity measurements have also been widely used in the elucidation of formation of complexes. In the present work, we made an attempt to study the molecular interactions in binary mixtures using an empirical relation of intermolecular free length.

2. MATERIALS AND METHODS

The experimental data for the present work were adopted from the published paper of Roshan Abraham,M.Abdulkhadar and C.V.Asokan. The liquid mixtures chosen are

1. Methyl ethyl ketone(MEK)+methanol(ML)
2. Methyl phenyl ketone(MPK)+methanol(ML)

The detailed study of intermolecular free length (L_f) in liquids were done by Bertil Jacobson and he derived the equation.

$$L_f = K\sqrt{\beta}_{ad}$$

$$L_f = \frac{K}{U\rho^{\frac{1}{2}}} \tag{1}$$

where U is the sound velocity and ρ is the density of the liquid. K is called Jacobson constant.

Since U and ρ are the temperature sensitive parameters, on differentiating Equation (1) with respect to temperature gives

$$\frac{dL_f}{dT} = L_f(\frac{\alpha}{2} + \beta) \tag{2}$$

where

$$\alpha = \frac{-1}{\rho}(\frac{d\rho}{dT})_p,$$

is the temperature coefficient of density and

$$\alpha = \frac{-1}{U}(\frac{dU}{dT})_p,$$

is the temperature coeffcient of sound velocity. From equation (2)

$$\ln L_f = (\frac{\alpha}{2} + \beta)T + C \tag{3}$$

where C is the constant of integration. or

$$L_f = L'^f \exp(\frac{\alpha}{2} + \beta)\Delta T \tag{4}$$

Thus, if we know the intermolecular free length of a liquid at a lower temperature $(L_f^{'})$, we can determine the intermolecular free length of that liquid at any higher temperature (L_f), using the above equation

$$L_f = L'^f \exp(\frac{\alpha}{2} + \beta)\Delta T \tag{5}$$

3. RESULTS AND DISCUSSION

The variation of intermolecular free length (L_f) with mole fraction (x) for the binary mixture methyl ethyl ketone (MEK) and methanol (ML) at 313K is shown in Figure 1. The value of $L_f$decreases with increase in mole fraction for both experimental and theoretical cases. It can be seen that the deviation of experimental and calculated values of$L(L_f^E = L^{expt} - f_f^{calc})$ increases with increase in mole fraction.

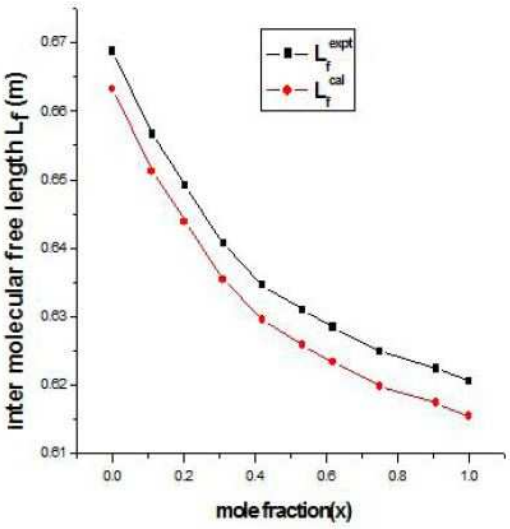

Figure 1. Variation of L_f^{expt} and$L_f^{cal}$for the binary mixture Methyl ethyl ketone and Methanol with mole fraction at temperature 313 K.

Figure 2 shows the variation ofL_f with mole fraction of the same mixture at 323K.Here also the magnitude of L_f decreases with increase in mole fraction and the excess values increases with increase in mole fraction. For methyl phenyl ketone (MPK) and methanol (ML) mixture at $313K$, the value ofL_f decreases with increase in mole fraction and the excess values also increases with

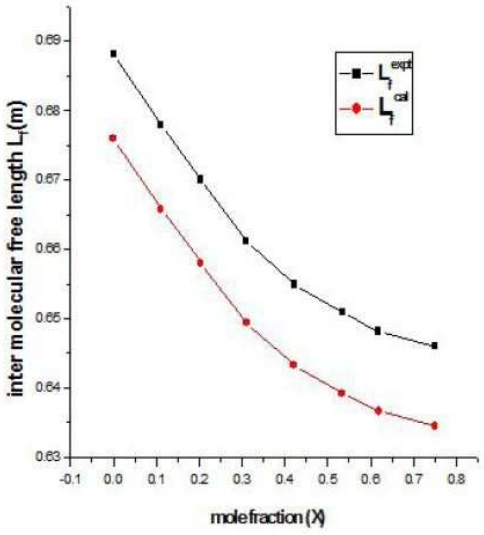

Figure 2. Variation of L_f^{expt} and$L_f^{cal}$for the binary mixture Methyl ethyl ketone and Methanol with mole fraction at temperature 323 K.

increase in mole fraction. But the deviation between experimental and calculated values is less when compared to MEK+ML mixture. This is shown in Figure 3.

At $323K$, the value ofL_f decreases with increase in mole fraction and the excess values also increases with increase in mole fraction. But the deviation between experimental and calculated values is less when compared to MEK+ML mixture. This is shown in Figure 4.

On analyzing the above graphs, it can be seen that for both the liquid mixtures at the chosen temperatures, the excess values ofL_f increases with increase in temperature and concentration. Also it is evident from the graphs of both the binary mixtures that the excess values ofL_f are positive through- out the concentration range. The magnitude of excess values increases with increase in temperature.

4. CONCLUSION

The intermolecular free length (L_f) is an important physical property of liquid mixtures which mainly affects the sound velocity in liquids. The in- termolecular free length increases with increase of temperature and hence the close packing of molecules which in effect decreases the sound velocity. The excess thermodynamic parameters such as excess adiabatic compress- ibility (β_s^E) and excess intermolecular free length (L_f^E) are very useful in understanding the intermolecular interactions in binary mixtures.

When negative excess functions are observed, complex formation is sus- pected more often.

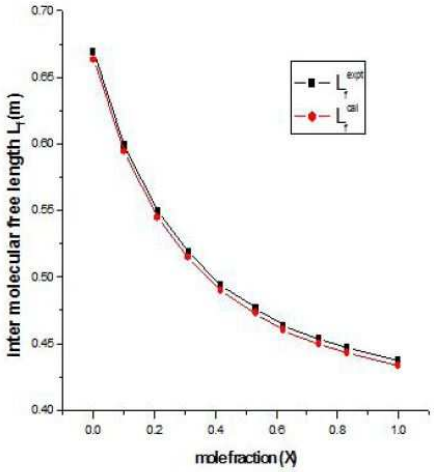

Figure 3. Variation of L_f^{expt} and$L_f^{cal}$for the binary mixture Methyl phenyl ketone and Methanol with mole fraction at temperature 313 K.

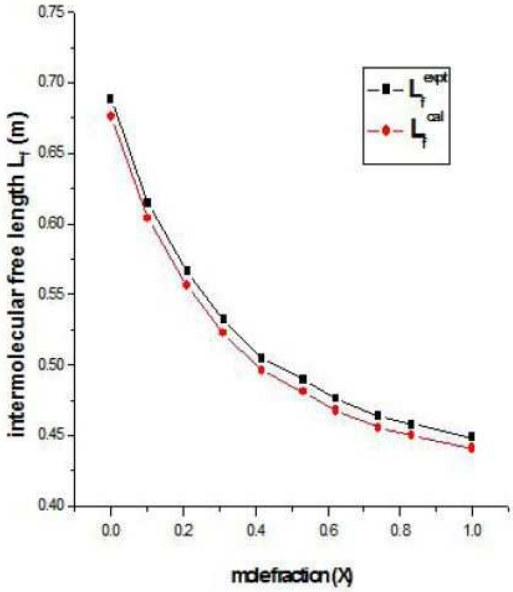

Figure 4. Variation of L_f^{expt} and$L_f^{cal}$for the binary mixture Methyl phenyl ketone and Methanol with mole fraction at temperature 323 K

This suggests the occurrence of discrete groups of molecules arranged into specific geometric structures. These structural arrangements are influenced not only by the shape of the molecules but also by their mutual interactions. The positive values in excess properties correspond mainly to the existence of dispersion forces. These derived parameters offer a conve- nient method for the study of thermodynamic properties of liquid mixtures which are not easily obtained by other means.

In the present work, close examination of the graphs show that the inter molecular free length increases with temperature in all the mixtures, which leads to increase in adiabatic compressibility. So, the increase of intermolecular distance increases the distance between the surface of the two molecules. The excess values of L_f is positive throughout the concentration range for all the binary mixtures chosen. This suggests the presence of molecular interaction in the present mixtures which may be due to dispersion forces.

References

[1] Roshan Abraham, M.Abdhulkhadar and C.V.Asokan, Acoustics Letters Vol. 20, 1997.

[2] Bertil Jacobson, Acta Chemica Scandinavica (1952).

[3] C.Shanmuga Priya, S.Nitya, G.Velraj and A.N.Kanappan, International Journal of Advanced Science and Technology Vol.18, 2010.

[4] S.Prabakar and K.Rajagopal, Pure and Applied Ultrasonic Vol. 27, 2005.

[5] D.Panday, Vinay Sanguri, M.K.Yadav and Aruna Singh, Indian Journal of Chemistry Vol.47A, 2008.

[6] Harish Kumar and Deepika, International Journal of Chemical Science And Technology, 2012.

[7] Ranjith Kumar Bachu *et. al.*, International Journal of Chemical Science and Technology, Vol 47A, 2008.

[8] Saravanakumar K and Kubendran T.R, Research Journal of Chemical Sciences Vol. 2(4), 50-56, April (2012).

[9] Bojan D. Djordjevi *et. al.*, journal of the Serbian Chemical Society, Vol 74(5), 2011.

[10] Savitha Jyostna Tangeda and Satyanarayana, Indian Journal of Chemical Technology, Vol 13, 2006.

[11] T.R Kubendran, Modern Applied Science, Vol 2(3), 2008.

[12] J.N.Ramteke, Advances in Applied Science Research, Vol.3(3), 2012.

Study of Temperature and Concentration Dependence of Refractive Index of Various Liquids using a Simple Technique of Laser Refraction

Sarthak Mohapatra[†], Somadutta Bhatta[‡] and Pravakar Pradhan[§*]
[†]CET,Bhubaneswar, [‡]NISER,Bhubaneswar,[§]Ravenshaw University,Cuttack

Abstract. Refractive Indices of liquid materials of various concentration at different temperatures has been measured by a simple but innovative method using a LASER beam.The measured data has been compared with the available data measured through various other complex techniques.This study confirms the validity of our simple technique which can be adopted for various purposes.

Communicated by: L. Satpathy

1. INTRODUCTION

As long as light travels in a straight line it is beautiful but when light bends it is wonderful.The bending of light as it crosses the interface between two materials constitutes the most fundamental optical effect "REFRACTION". Every material including air has an index of refraction (or Refractive Index). Refractive index is one of the most basic optical properties of the medium. The refractive index of a medium differs with frequency of light used. This effect known as dispersion, let expansion coefficient[1]. The refractive index has also been used as a tool for finding the adulteration of oils[2]. A simple approximation of the dependence of refractive index of water on temperature and wavelength in the spectral range from 200 to 1000 nm has been found to be important for different applications in biomedical optics of tissues[1].

In the above mentioned studies, several techniques are reported in literature for measurement of refractive index of liquids. However, the technique seems to be quite complicated and need more sophisticated instruments like optical spectrometer, grating, hollow prism etc. The advent of low cost lasers like laser-pointer, laser levels allows us to experimentally measure the values of refractive indices of various liquids. The low cost and simple method we proppose here involves only the principle of reflection and refraction to determine the refractive indices of variousliquids instantly. Morever the arrangement is easy and very small amount of liquid is required for the experiments. So it can be used in various industries to determine the refractive index of cheap as well as very expensive liquids like expensive paints, medicines, spacecraft fuel etc. which are usually in the form of liquid and their optical phenomena are ought to be studied. This experiment can also be included in the undergraduate syllabus for the study of refraactive index of liquids.

*[†]sarthakmohapatra1995@yahoo.co.in,[‡] som.bhatta@niser.ac.in

We have given a detailed derivation of formula and ray diagram for calculating refractive index of liquid from the observed data.We have experimentally measured the refractive index of:

- ater at different temperatures
- copper sulphate ($CuSo_4$) salt solution at various % of concentrations.
- potassium chloride (KCl) salt solution at various % of concentrations.
- sucrose solution at various % of concentrations.
- common salt solution at various % of concentrations.
- glycerine at room temperature.

Our experimental data has been graphically commpared with the measured data of other methods.The exceelent agreement of our data supports the validity of our experimental procedure,and can be improvised and extended for many other liquid.

2. DERIVATION OF FORMULA

2.1 *Principe*

The experiment is based on the principle of LAWS OF REFLECTION and LAWS OF REFRACTION of light. Let us assume Angle of incidence=θ and Angle of refraction =α. Using Snell's

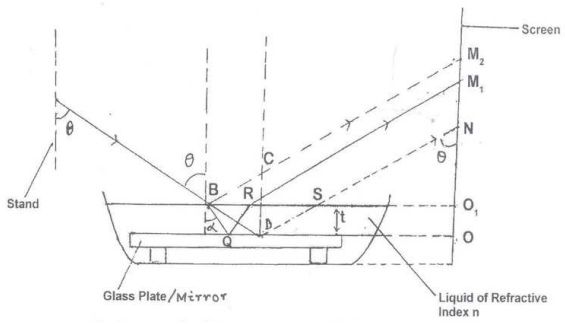

Figure 1. Schematic Diagram of experimental setup.

law,

$$n_1 \sin\theta = n_2 \sin\alpha \tag{1}$$

$$\Rightarrow n_2 = n_1(\sin\theta/\sin\alpha) \tag{2}$$

where, n_1 = Refractive index of air, n_2 = Refractive index of liquid. In $\triangle$ ODN, $\angle$ OND = θ (Because BM_2,DN are parallel and BD is transversal) so,

$$\tan\theta = \frac{OD}{ON} \tag{3}$$

In $\triangle$ BDS,

$$BS = 2t(\tan\theta) \tag{4}$$

where t is the thickness/depth of the liquid. Similarly, from $\triangle BQR$,

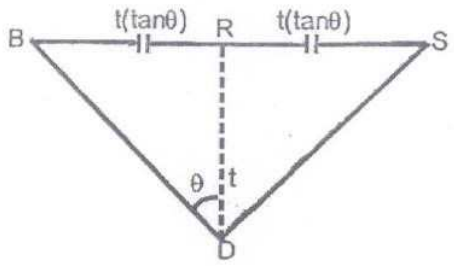

Figure 2.

$$BR = 2t(\tan\alpha) \tag{5}$$

From $\triangle O_1SN$ and $\triangle O_1BM_2$,

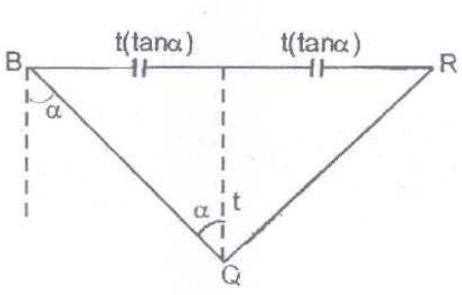

Figure 3.

$$O_1S = O_1N\tan\theta \tag{6}$$

$$O_1B = O_1M_2\tan\theta \tag{7}$$

From equation 5 and 6; we have

$$O1_B - O_1S = (O_1M_2 - O_1N)\tan\theta = BS = NM_2\tan\theta \tag{8}$$

Comparing equation (3) and equation (6),

$$2t(\tan\theta) = NM_2(\tan\theta) \tag{9}$$

$$\Rightarrow 2t = NM_2 \tag{10}$$

Now,From equation(4);

$$\tan\alpha = \frac{BR}{2t} \tag{11}$$

$$= \frac{O_1B - O_1R}{2t} \tag{12}$$

$$= \frac{(O_1M_2 - O_1M_1)\tan\theta}{2t} \tag{13}$$

$$= \frac{M_2M_1\tan\theta}{2t} \tag{14}$$

Using equation(2) for $\tan\theta$ and equation (10) for $2t$,we get;

$$\tan\alpha = M_2M_1\frac{(}{OD}ON)\frac{1}{NM_2} \tag{15}$$

Using equation (2)and equation(15) in equation (2),and assuming $n_1 = 1$,we have;

$$n_2 = \frac{\sin\theta}{\sin\alpha} \tag{16}$$

$$= \frac{\sin(\tan^{-1}\frac{OD}{ON})}{\sin(\tan^{-1}(\frac{M_2M_1}{NM_2})\frac{OD}{ON})} \tag{17}$$

Let $OD = x$, $ON = y$, $M2M1 = u$, $NM2 = v$

so,

$$n_2 = \frac{\sin[\tan^{-1}\frac{x}{y}]}{\sin[\tan^{-1}\frac{ux}{vy}]} \tag{18}$$

$p = ux$ and $q = vy$; so,

$$n = \frac{\frac{x}{\sqrt{x^2+y^2}}}{\frac{p}{\sqrt{p^2+q^2}}} \tag{19}$$

$$\Rightarrow n = \frac{x\sqrt{p^2+q^2}}{p\sqrt{x^2+y^2}} \tag{20}$$

$$\Rightarrow n = \sqrt{\frac{1+\frac{q^2}{p^2}}{1+\frac{x^2}{y^2}}} \tag{21}$$

$$\Rightarrow n = \sqrt{\frac{1+\frac{y^2v^2}{u^2x^2}}{1+\frac{x^2}{y^2}}} \tag{22}$$

So,we get,

$$n_2 = N_{liquid} = \sqrt{\frac{1+\frac{y^2v^2}{u^2x^2}}{1+\frac{x^2}{y^2}}}$$

3. EXPERIMENTAL SETUP

3.1 *Equipments*

In the present experimental setup we have studied the temperature and concentration dependence of refractive index of various liquids by the help of a simple technique.For this purpose mainly we are using the following equipments to carry out the experiment.They are:

1. A Petri dish
2. small piece of mirror
3. A laser light
4. A sheet of graph paper
5. liquids

3.2 *Construction*

• A mirror is placed in the petridish and the dish is placed on the table as shown in the Figure 4.

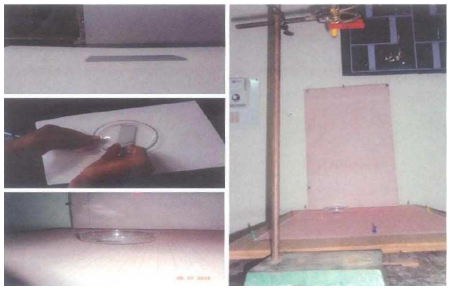

Figure 4. Experimental setup for conducting experiments

• The mirror must be perfectly horizontal as verified with a spirit level.We use water proof glue under the mirror to level it.
• An ordinarily laser torch is mounted on a stand with protractor to measure the angle.The stand is kept on one side of the disc.

• On the other side of the disc,a sheet of graph paper was mounted on a stand which acts as a screen.
• The liquid whose refractive index is to be determined is kept ready as shown in Fig.5 below.

Figure 5. Filling of petridish with copper sulphate solution

3.3 *Working*

Figure 6. Refraction of laser through copper sulphate solution

• Light from laser torch is reflected off the surface of the mirror to produce a spot of light on the graph sheet,which is mounted on the stand and acts as a screen.
• The position of this spot is marked on the graph sheet with a pencil.
• The position of the spot which falls on the mirror is marked on the table. Let it be O.
• without disturbing any apparatus a little amount of liquid is poured into the petridish to make a

thin layer of the liquid on the mirror.
• The thickness of the liquid layer may vary from a few milimetres to a couple of centimetres.
• We then get two spots appearing on the wall:one from the beam which is reflected from the liquid surface(M_2) and other from the beam which reflects through the liquid from the mirror(M_1) as shown in the Figure 1.
• When the spots are clearly visible on the screen then only we mark the spots properly as shown in the Figure 6. • The horizontal separation from the initial point D to the screen O is OD .Let OD=x.
• The vertical distance of separation between the two point O to N is ON. Let ON=y.
• The vertical distance of separation betwen two points of separation between the two points M_2 to M_1 is M_2M_1. Let $M_2M_1 = u$.
• The vertical distance of separation between the two points N to M_2 is NM_2. Let NM_2=v.
• We calculate the refractive index of the liquid by using the formula given by equation no 14.
• This is repeated for number of liquids at various temperatures and for various concentration.

3.4 *Example*

a) If glycerine is taken as experimental liquid then we get the following picture on the screen (Fig. 7).
b) If hot water is taken as the liquid then we get the following picture on the screen (Fig. 8).

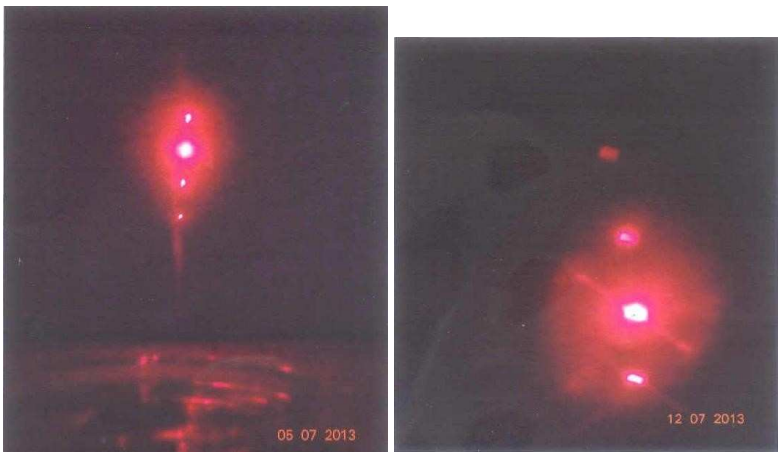

Figure 7. Refraction of laser through copper sulphate solution

Figure 8.

4. RESULTS AND DISCUSSIONS

4.1 *For Copper Sulphate solution*

Table 1. Copper Sulphate Solution

concentration (in%)	Refractive Index(n)
5	1.242
10	1.333
15	1.348
20	1.364
25	1.371

The graph shows sharp increase of refractive index as the % of concentration of salt increases from 5% to 10%.Beyond 10% refractive index varies smoothly.

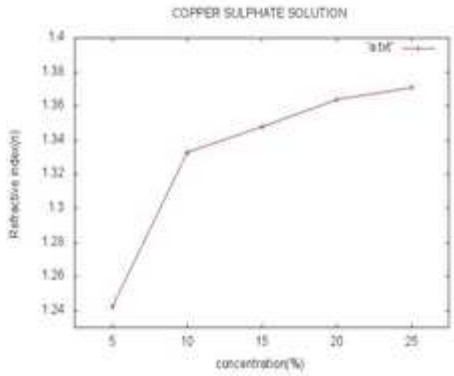

Figure 9. Refractive index of copper sulphate solution as a function of its concentration expressed in percentage

4.2 *For Hot water*

As expected, the graph indicates that the refractive index of water decreases as temperature increases.

4.3 *For Common Salt Solution*

In common salt refractive index varies/increases smoothly with increase of concentration.

Table 2. (Hot water)

Temperature(in ^{o}C)	Refractive Index(n)
40	1.325
50	1.312
60	1.301
70	1.289
80	1.275

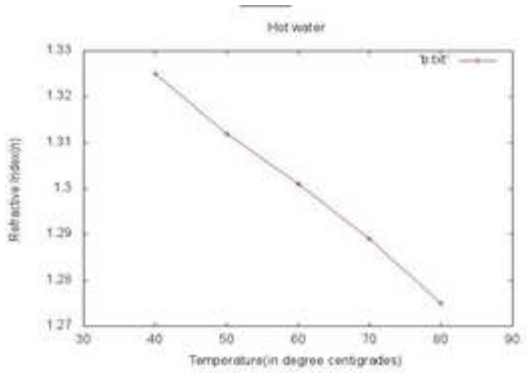

Figure 10. Temperature dependence of refractive index of hot water

Table 3. (Common Salt solution)

Concentration(in %)	Refractive Index(n)
2.5	1.330
5	1.335
10	1.343
15	1.349
20	1.353

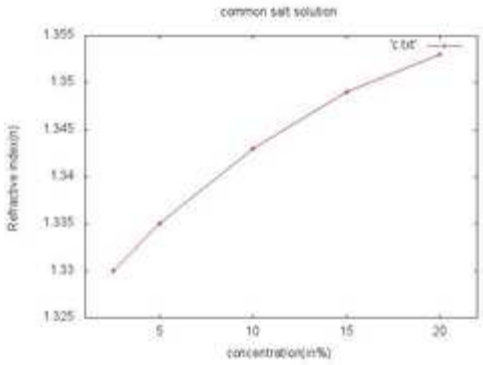

Figure 11. Refractive index of common salt as a function of its concentration expressed in percentage

4.4 *Sucrose solution*

The variation of refractive index of sucrose with concentration has been compared with the available data in literature.The graph shows excellent agreement with literature value in higher concentration.However,the pattern looks almost similar in both cases.The smoothness of variation in $CuSO_4$ and sucrose at higher concentrations can be attributed to the exothermic nature of the salts.

Table 4. (Sucrose solution)

Concentration(in %)	Refractive Index(n)	Literature value
5	1.332	1.340
10	1.337	1.345
15	1.343	1.355
20	1.356	1.360
40	1.392	1.395

4.5 *For Potassium Chloride*

Table 5. (Potassium Chloride solution)

Concentration(in %)	Refractive Index(n)	Literature value
2.5	1.336	1.332
5	1.341	1.338
10	1.350	1.346
15	1.355	1.351
20	1.363	1.360

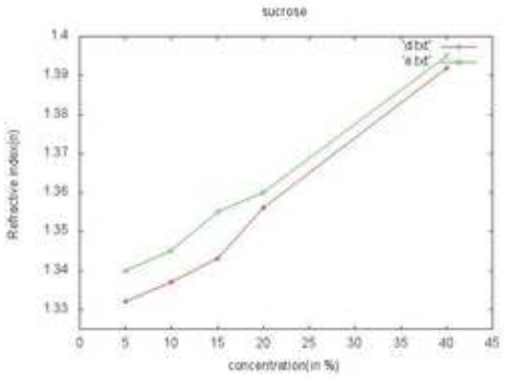

Figure 12. Refractive index of sucrose as a function of its concentration measured by the present technique and obtained from literature (e.txt-literature value;d.txt-present technique)

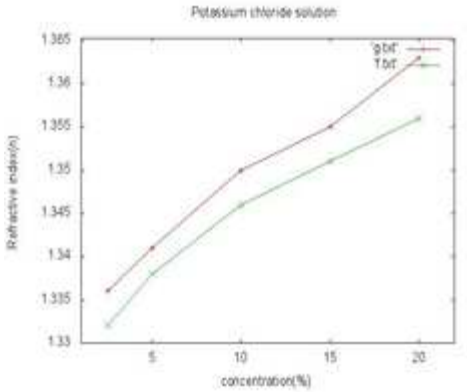

Figure 13. Refractive index of Potassium chloride as a function of its concentration measured by the present technique and obtained from literature(g.txt-present technique;f.txt-literature value))

5. CONCLUSION

The present profile of experimental results show that,this simple laboratory technique could be safely employed to study the dependence of refractive index of solution on their concentration as well as on the temperature.From this experimental study a linear dependence of refractive index of some solutions with their concentration has been observed.The temperature coefficient of refractive index of hot water and the refractive index of the concentration of the soilution,was determined and it

was found to be in agreement with the results obtained from other methods of meaurements.This confirms the validity of experimental procedure for wide range of liquid at different temperature and concentration.Morever,this experimental setup is very low cost,convenient to handle at the school/college level laboratory,hence has advantage over other experimental procedure cited in literature.This method also reveals that it can be used as a quality control technique such as adulteration of oils,fuels like,diesel,petrol and medicine by measuring the refractive index of such liquid materials. Since this technique is simple it can be included as an experimental verification in school level laboratory manual and can be conducted in short time where any such procedure of refractive index of liquid is hardly found.

References

[1] Alexy N. Bashkatov,Elina A. Genia, "Water refractive index in dependence on temperature and wavelength: A simple approximation", Proc. of SPIE, Vol.5068, 2003.

[2] Aripponalmmal S., "A Novel method of using refractive index as a tool for finding adulteration of oils", Res. J. Recent Sci., Vol-1, No.7, 77-79, July, 2012.

[3] D.J Kumar, P.K. and Naresh Jolly,"Refractive index of liquids using Laser light",Lab Experiments, Vol-8, No.3 Sept. 2008.

[4] Grzegorz F. Wojewoda,"Measuring index of refraction", hanson@ups.edu

[5] Maria C. Velazquez. Ahumadaetal., "Demonstration of negative refraction of microwaves", Am. J. Physics, Vol-79, No.4, April-2011.

[6] Subedi D.P., Adhikari D.R., Joshi U.M., Poudel H.N., Niraula .B, "Study of temperature and concentration dependence of refractive index of liquids using a novel technique", Vol-II, No.1, February 2006.

[7] Singh S. Physics Education, PP 152-153, March 2002.

Calculation of Extremal Black Hole Entropies

P.K. Adithya and Prashant Kocherlakota
4^{th} year B.Tech. (Engineering Physics), Department of Physics, Indian Institute of Technology Madras, Chennai 600 036, India.

Abstract. We discuss the importance of attractor mechanisms and of entropy functions of black holes and the various insights they provide. We describe the process of extremizing entropy functions for extremal black holes 3+1 dimensions and demonstrate this process by considering the Gauss-Bonnet correction to the standard Einstein-Maxwell entropy function and then extremizing it in 3+1 dimensions. We generalize this procedure to compute the black hole entropy in a more general higher derivative gravitational system.

Communicated by: L. Satpathy

1. BLACK HOLES - AN INTRODUCTION

Black holes are objects that are characterised by a complete collapse of matter. A sufficiently massive object that is unable to resist its own gravitational pull undergoes disastrous gravitational collapse to result in an object whose gravity is so strong that nothing can escape from it. Around a black hole there is a mathematically defined surface called an event horizon that marks the point of no return. A black hole is characterized completely by its event horizon.[1]

An important property of black holes is the no-hair theorem. An astrophysical object like the earth or the sun has a structure that could well be non-homogeneous. For example, the earth is actually an oblate spheroid, and has non-uniformities like mountain peaks and craters. This is reflected in the fact that the earth's gravitational field is not perfectly spherically symmetric about it. However, that is not the case when it comes to a black hole. Though the star which collapsed gravitationally to form the black hole could have "had hair", the black hole itself does not.

The above result means that a black hole is completely specified by its mass, spin and charge. In this respect, it is very much like an elementary particle. If we were to conclude that a black hole is thus a very simple object, we would be correct as far as classical general relativity can take us. However, black holes also have a huge value of entropy. In fact, the entropy of a black hole is much bigger than the entropy of a star that might have collapsed to form it. Since entropy is directly related to the number of possible micro-states by Boltzmann's formula, the high value of a black hole's entropy points to a complex micro-structure. In this regard, it is very different from a particle.

Understanding the complex micro-structure of a black hole implied by its entropy is an important problem in quantum gravity. Now we understand that the apparent simplicity of a black

[1] For more detail description of black holes, see, for example [1, 2].

hole is not because it is like a structure-less elementary particle, but because of its resemblance to a statistical ensemble .

2. BLACK HOLE GEOMETRIES

The simplest action that we consider in General Relativity is the Einstein-Maxwell action, given by:

$$\frac{1}{16\pi G}\int R\sqrt{g}d^4x - \frac{1}{16\pi}\int F^2\sqrt{g}d^4x$$

Here, g and R are respectively the determinant and the Ricci scalar of the metric $g_{\mu\nu}$. $F_{\mu\nu}$ is the electromagnetic field tensor and $F^2 = F_{\mu\nu}F^{\mu\nu}$. G is Newton's gravitational constant.

In the absence of any electric or magnetic charges, as well as any other matter fields, the Euler-Lagrange equations are the Einstein field equations for free space, i.e.:

$$R_{\mu\nu} - \frac{1}{2}g_{\mu\nu}R = 0$$

This has many solutions, the flat spacetime Minkowski metric being one of them, of course. However, we are interested in analysing the geometry of the spacetime around a black hole. According to general relativity, in a given spacetime, free particles always move along geodesics - curves of extremal lengths between two given points. Geodesics are the natural generalisation of straight lines in a Euclidean geometry. So we try to choose a solution such that the geodesic equations in this geometry reduce to the equations of motion that one would obtain by using Newton's laws of motion in the Newtonian limit (i.e., the limit of small velocities). This leads us to what is known as the Schwarzschild solution. It can be shown that the desired geometry is given by the Schwarzschild metric:

$$ds^2 = -\left(1 - \frac{2GM}{r}\right)dt^2 + \left(1 - \frac{2GM}{r}\right)^{-1}dr^2 + r^2d\Omega^2$$

Here, t is time, r is the radial coordinate and Ω is the solid angle on a 2-sphere.

This solution appears to have a singularity at $r = 2GM$, for which the metric component g_{tt} vanishes, and g_{rr} appears to blow up, but it is in fact a mere coordinate singularity, appearing because of our naive choice of coordinates. The surface $r = 2GM$ is called the event horizon of the black hole. A lot of the interesting physics associated with a black hole happens in and around its event horizon.

3. TEMPERATURE AND ENTROPY OF A BLACK HOLE

The laws of black hole thermodynamics appear to be a recast version of the classical laws of thermodynamics in terms of the surface gravity and the black hole horizon radius. The question of a black holes entropy was first raised by Jacob Bekenstein, who pointed out that if a black hole did not have any entropy, then tossing an object with finite entropy into it would cause the entropy of

the universe to decrease. It had to follow that the black hole carried an entropy, which Bekenstein hypothesised was proportional to its area.

However, this would mean that the black hole also has a temperature, given by

$$\frac{1}{T} = \frac{\partial S}{\partial E}$$

If a black hole has a finite temperature, then it must radiate. However, this is impossible for a classical black hole, for reasons given above.

Stephen Hawking resolved this paradox by showing that once quantum effects are taken into account, it is possible for radiation to be emitted from a black hole. In quantum theory, pairs of virtual quanta are continually created in pairs in the vacuum, and then annihilate back into the vacuum. Typical virtual quanta with wavelength of order λ can separate by a distance of order λ before they must recombine and annihilate. However, it may happen that one of the particles is behind the event horizon while the other is outside it. In this case, an observer outside the event horizon will never see the annihilation (because one cannot see an object disappearing into a black hole - it will only appear to asymptotically reach the event horizon) and has no choice but to interpret the particle that he does see as a real quantum of radiation.

In fact, Hawking's calculations showed that the spectrum of a black hole corresponds to that of a black body of temperature $T = \frac{\hbar\kappa}{2\pi} = \frac{\hbar}{8\pi GM}$. From this, using the First Law, it can be shown that the entropy of a black hole is $S = \frac{Ac^3}{4G\hbar}$.

This finite value of entropy naturally raises the question about the microstates that account for it. The entropy is hence a valuable piece of information that a quantum theory of gravity must corroborate.[2]

4. ENTROPY CALCULATIONS FOR EXTREMAL BLACK HOLES

One of the greatest triumphs of string theory has been to reproduce the black hole entropy result from a statistical calculation for a class of black holes known as extremal black holes. These black holes have zero temperature, and hence do not emit Hawking radiation and are stable. They may also be invariant under supersymmetry transformations. These two facts give us a foothold and allow us to calculate the degeneracy of such states at weak coupling, where the gravitational backreaction of the system can be ignored. It turns out that this calculation gives precisely the same result, in the limit of large charges where the contribution of higher derivative terms in the effective action of string theory can be ignored.

Given this success, it is natural that we want to see how far we can test this corroboration. When we move away from the large charge limit, the curvature and other field strengths at the horizon are no longer negligible. Typical examples of such higher derivative terms are terms involving squares and higher powers of the Riemann tensor. For a large but finite size black hole we expect the

[2]For a description on quantum black holes, see the review article[3].

effect of these higher derivative terms at the horizon to be small but non-zero, giving rise to small modifications of the horizon geometry and consequently the black hole entropy.

There are several technical complications that arise when we make such an attempt, but a brief outline of the calculation will be presented here. We closely follow the convention and system used by Sen[4, 5].

From the Einstein-Maxwell action, we can derive the Reissner-Nordstrom solution, which gives us the field configuration that extremise the action, i.e., the values of the metric and the electromagnetic field tensor. This field configuration is parametrised by the electric and magnetic charge of the black hole and its mass. It has two horizons, an inner one and an outer one. However, we can choose the mass such that the radii of the inner and outer horizons coincide. The near horizon geometry of such a black hole then turns out to be $AdS_2 \otimes S^2$ (in four dimensions), and this geometry has $SO(2,1) \times SO(3)$ isometry.

It turns out that all known extremal spherically symmetric black holes in four dimensions with nonsingular horizon have near horizon geometry $AdS_2 \otimes S^2$ and an associated isometry $SO(2,1) \times SO(3)$. We shall take this as the definition of an extremal black hole, even in the presence of higher derivative terms.

Let us consider a theory of gravity coupled to some Abelian gauge fields $A_\mu^{(i)}$ and neutral scalar fields $\{\phi_s\}$. Let $\sqrt{-detg}L$ be the Lagrangian density, expressed as a function of the metric $g_{\mu\nu}$, the scalar fields $\{\phi_s\}$, and the gauge field strengths $F_{\mu\nu}^{(i)}$, and the covariant derivatives of these fields.

We consider a spherically symmetric extremal black hole solution consistent with $SO(2,1) \times SO(3)$ isometry. The most general field configuration consistent with this is of the form:

$$ds^2 \equiv g_{\mu\nu}dx^\mu dx^\nu = v_1(-r^2dt^2 + \frac{dr^2}{r^2}) + v_2(d\theta^2 + \sin^2\theta d\phi^2)$$

$$\phi_s = u_s$$

$$F_{rt}^{(i)} = e_i, F_{\theta\phi}^{(i)} = \frac{p_i}{4\pi}\sin\theta$$

Here, v_1, v_2, $\{e_i\}$, $\{p_i\}$ and $\{u_s\}$ are constants.

Let us define a function $f(\vec{u}, \vec{v}, \vec{e}, \vec{p})$ given by:

$$f(\vec{u}, \vec{v}, \vec{e}, \vec{p}) = \int d\theta d\phi \sqrt{-detg}L$$

The constants p_i correspond to magnetic charges carried by the black hole, and also that $\frac{\partial f}{\partial e_i} = q_i$, where q_i are the electric charges carried by the black hole.

The entropy function, $\varepsilon(\vec{u}, \vec{v}, \vec{e}, \vec{q}, \vec{p})$, is defined by:

$$\varepsilon = 2\pi(e_i q_i - f)$$

The value of the entropy of the black hole is the value of the entropy at its extremum, obtained by extremising ε with respect to u_s, v_s and e_i. The final result is a value that depends only on the

electric and magnetic charges of the black hole, which is consistent with our initial procedure of defining an extremal black hole.

Now we shall see a few examples of higher derivative corrections to the string theory effective action and calculate the corrections to the entropy.

5. ENTROPY CORRECTIONS DUE TO GAUSS-BONNET TERMS

In higher derivative gravity, the most general Lagrangian (known as the Lovelock Lagrangian [6])is a polynomial of the Riemann tensor, involving squares and its higher powers. However, it can be shown that in four spacetime dimensions, the only non-trivial correction is the Gauss-Bonnet term, which involves squares of the Riemann tensor. All other terms will become total derivatives and not contribute to the dynamics. We introduce a Gauss-Bonnet term in the Lagrangian, given by:

$$\Delta L = \phi(a,S)(R_{\mu\nu\rho\sigma}R^{\mu\nu\rho\sigma} - 4R_{\mu\nu}R^{\mu\nu} + R^2) \tag{1}$$

The correction to the entropy function is then given by

$$\Delta\varepsilon = -2\pi \int d\theta d\phi \sqrt{-det\ g}\Delta L$$

evaluated on the horizon.

Now, any extremal black hole has an $AdS_2 \otimes S^2$ geometry on the horizon, i.e., the near-horizon geometry factors out into a two-dimensional Anti de Sitter space and a 2-sphere.

$$ds^2 = v_1\left(-r^2dt^2 + \frac{dr^2}{r^2}\right) + v_2\left(d\theta^2 + \sin^2\theta d\phi^2\right) \tag{2}$$

We now go about finding the Riemann and Ricci curvature tensors, for which we have to first evaluate the Christoffel symbols. Since the geometry has been factorised, it can be concluded that the value of a Christoffel symbol will be zero whenever all the indices do not belong to one of the factors.

$$\Gamma^{\alpha}_{\ \mu\nu} = \frac{1}{2}g^{\alpha\beta}\left(\partial_\nu g_{\mu\beta} + \partial_\mu g_{\nu\beta} - \partial_\beta g_{\mu\nu}\right) \tag{3}$$

From this, it can be seen that the only non-zero Christoffel symbols for the AdS_2 part are $\Gamma^{t}_{\ tr} = \Gamma^{t}_{\ rt} = \frac{1}{r}$, $\Gamma^{r}_{\ tt} = r^3$ and $\Gamma^{r}_{\ rr} = \frac{-1}{r}$. Similarly, the only non-zero Christoffel symbols for the 2-sphere are $\Gamma^{\theta}_{\ \phi\phi} = -\sin\theta\cos\theta$ and $\Gamma^{\phi}_{\ \theta\phi} = \Gamma^{\phi}_{\ \phi\theta} = \cot\theta$.

Once we have the Christoffel symbols, we can calculate the Riemann tensor components. Again, a Riemann tensor component will be zero if all the indices do not belong to one of the geometry factors. By further antisymmetry considerations, we can reduce the number of independent components of $R_{\mu\nu\rho\sigma}$ to two - namely, R_{rtrt} and $R_{\theta\phi\theta\phi}$.

$$R^{\rho}_{\ \sigma\mu\nu} = \partial_\mu\Gamma^{\rho}_{\ \sigma\nu} - \partial_\nu\Gamma^{\rho}_{\ \sigma\mu} + \Gamma^{\rho}_{\ \mu\lambda}\Gamma^{\lambda}_{\ \sigma\mu} - \Gamma^{\rho}_{\ \nu\lambda}\Gamma^{\lambda}_{\ \mu\sigma} \tag{4}$$

From this, we can calculate that $R^r{}_{trt} = r^2$ and $R^\theta{}_{\phi\theta\phi} = \sin^2\theta$.

$$R_{rtrt} = g_{rr}R^r{}_{trt} = v_1$$

$$R_{\theta\phi\theta\phi} = g_{\theta\theta}R^\theta{}_{\phi\theta\phi} = v_2\sin^2\theta$$

Similarly, we can find the completely contravariant forms of the Riemann tensor with appropriate use of the metric. We can now evaluate the first term of the Gauss-Bonnet Lagrangian and it turns out as follows.

$$R_{\mu\nu\rho\sigma}R^{\mu\nu\rho\sigma} = 4\left(\frac{1}{v_1^2} + \frac{1}{v_2^2}\right)$$

The factor of four comes in because there are actually four non-zero components of the Riemann tensor in each of the factor geometries (though only one independent component). Next, we need to find the Ricci tensor components.

$$R_{\mu\nu} = R^\rho{}_{\mu\rho\nu} \tag{5}$$

From this, we can see that the non-zero components of the Ricci tensor are the diagonal ones, i.e., R_{tt}, R_{rr}, $R_{\theta\theta}$ and $R_{\phi\phi}$.

$$R_{tt} = R^r{}_{trt} = r^2$$

$$R_{rr} = R^t{}_{rtr} = g^{tt}R_{trtr} = -\frac{1}{r^2}$$

$$R_{\theta\theta} = g^{\phi\phi}R_{\phi\theta\phi\theta} = 1$$

$$R_{\phi\phi} = R^\theta{}_{\phi\theta\phi} = \sin^2\theta$$

Again, we can calculate the components of the completely contravariant form of the Ricci tensor and we are now ready to evaluate the second term of the Lagrangian.

$$-4R_{\mu\nu}R^{\mu\nu} = -8\left(\frac{1}{v_1^2} + \frac{1}{v_2^2}\right) \tag{6}$$

Now the last quantity we need to calculate is the scalar curvature.

$$R = g^{\mu\nu}R_{\mu\nu} \tag{7}$$

With this, the final term of the Lagrangian can be evaluated.

$$R = 2\left(-\frac{1}{v_1} + \frac{1}{v2}\right)$$

$$R^2 = 4\left(\frac{1}{v_1^2} + \frac{1}{v_2^2} - \frac{2}{v_1v_2}\right)$$

Hence, the value of the Lagrangian on the horizon is:

$$\phi(a,S)(R_{\mu\nu\rho\sigma}R^{\mu\nu\rho\sigma} - 4R_{\mu\nu}R^{\mu\nu} + R^2) = -\frac{8}{v_1v_2}\phi(a,S)$$

Now, we calculate the correction to the entropy.

$$\Delta\varepsilon = -2\pi \int d\theta d\phi \sqrt{-det\ g}\Delta L = -2\pi \int d\theta d\phi v_1 v_2 \sin\theta. - \frac{8}{v_1 v_2}\phi(a,S)$$

$$\Delta\varepsilon = 64\pi^2\phi(a,S) \tag{8}$$

Thus, we have found the correction to the entropy due to a Gauss-Bonnet term in the Lagrangian. It turns out to be independent of the sizes of the two geometries.

6. ENTROPY FUNCTION IN HIGHER DERIVATIVE GRAVITY

In this section, we consider a more general higher derivative Lagrangian as a substitute to the Einstein Hilbert action. This Lagrangian appeared in [7] in a different context as counter term in giving a description about c-theorem in arbitrary dimensions. Because of its rich structure we use it as a generalization to the Einstein Hilbert action and find the entropy function that it gives rise to. The Lagrangian is given by:

$$L = \frac{-2L^2}{l_p^2}\sqrt{-det(R_{ab} - \frac{1}{2}R\gamma_{ab} - \frac{1}{L^2}\gamma_{ab})} \tag{9}$$

The object γ_{ab} is given by the following relation:

$$G_{ab} = \frac{1}{2}\frac{d(d-1)}{L^2}\gamma_{ab}$$

In the above equation, G_{ab} is the Einstein tensor, defined by

$$G_{ab} = R_{ab} - \frac{1}{2}g_{ab}R$$

Now, we need to find the corresponding part of the entropy function by evaluating the following integral.

$$\varepsilon = -2\pi \int d\theta d\phi L \tag{10}$$

First we shall write down the components of the metric and the Ricci curvature tensors for the near horizon geometry, $AdS_2 \otimes S^2$, which we have already calculated.

$$R_{ab} = diag\left(r^2, -\frac{1}{r^2}, 1, \sin^2\theta\right)$$

$$R = g^{ab}R_{ab} = 2\left(-\frac{1}{v_1} + \frac{1}{v_2}\right)$$

We first need to calculate the Einstein tensor, which is clearly diagonal because both the metric and the Ricci tensor are diagonal. It can be easily shown, from the definition of the Einstein tensor, that:

$$G_{ab} = diag\left(\frac{v_1 r^2}{v_2}, \frac{-v_1}{v_2 r^2}, \frac{v_2}{v_1}, \frac{v_2\sin^2\theta}{v_1}\right)$$

We are now ready to evaluate the Lagrangian on the horizon, for which we first find the individual components of the tensor (call it Q_{ab}) whose determinant we are supposed to eventually take.

$$Q_{tt} = R_{tt} - \frac{1}{2}R\gamma_{tt} - \frac{1}{L^2}\gamma_{tt} = r^2\left(1 - \frac{1}{d(d-1)}\frac{v_1}{v_2}\left[L^2\left(\frac{-1}{v_1}+\frac{1}{v_2}\right)+1\right]\right) = r^2K_1$$

$$Q_{rr} = R_{rr} - \frac{1}{2}R\gamma_{rr} - \frac{1}{L^2}\gamma_{rr} = \frac{-1}{r^2}\left(1 - \frac{1}{d(d-1)}\frac{v_1}{v_2}\left[L^2\left(\frac{-1}{v_1}+\frac{1}{v_2}\right)+1\right]\right) = -\frac{1}{r^2}K_1$$

$$Q_{\theta\theta} = R_{\theta\theta} - \frac{1}{2}R\gamma_{\theta\theta} - \frac{1}{L^2}\gamma_{\theta\theta} = \left(1 - \frac{1}{d(d-1)}\frac{v_2}{v_1}\left[L^2\left(\frac{-1}{v_1}+\frac{1}{v_2}\right)+1\right]\right) = K_2$$

$$Q_{\phi\phi} = R_{\phi\phi} - \frac{1}{2}R\gamma_{\phi\phi} - \frac{1}{L^2}\gamma_{\phi\phi} = \sin^2\theta\left(1 - \frac{1}{d(d-1)}\frac{v_2}{v_1}\left[L^2\left(\frac{-1}{v_1}+\frac{1}{v_2}\right)+1\right]\right) = \sin^2\theta K_2$$

We have adopted the use of K_1 and K_2 for shorthand. Thus, the determinant of the tensor is the following.

$$det(Q_{ab}) = -\sin^2\theta K_1 K_2$$

where:

$$K_1(v_1, v_2) = \left(1 - \frac{1}{d(d-1)}\frac{v_1}{v_2}\left[L^2\left(\frac{-1}{v_1}+\frac{1}{v_2}\right)+1\right]\right)$$

$$K_2(v_1, v_2) = \left(1 - \frac{1}{d(d-1)}\frac{v_2}{v_1}\left[L^2\left(\frac{-1}{v_1}+\frac{1}{v_2}\right)+1\right]\right)$$

Now, the entropy function is:

$$\varepsilon = -2\pi\int d\theta d\phi L = \frac{16\pi^2L^2K_1K_2}{l_p^2}$$

The complete entropy function, including the electromagnetic Lagrangian contributions, is given by:

$$\varepsilon = 2\pi(qe - f) = 2\pi qe + \frac{16\pi^2L^2K_1K_2}{l_p^2} - 4\pi^2e^2\frac{v_2}{v_1} + 4\pi^2\left(\frac{p}{4\pi}\right)^2\frac{v_1}{v_2}$$

This function has to be extremised with respect to the electric field, e, and the sizes of the two geometries, v_1 and v_2.

Extremising with respect to the electric field first, we have:

$$\frac{\partial\varepsilon}{\partial e} = 0 \quad \Longrightarrow e = \frac{q}{4\pi}\frac{v_1}{v_2}$$

Substituting this back into the entropy function, we have:

$$\varepsilon = \frac{16\pi^2L^2}{l_p^2}K_1K_2 + \frac{1}{4}(q^2+p^2)\frac{v_1}{v_2}$$

We must remember that K_1 and K_2 are functions of v_1 and v_2, as defined above. Now we need to solve for values of v_1 and v_2 such that:

$$\frac{\partial\varepsilon}{\partial v_1} = 0, \frac{\partial\varepsilon}{\partial v_2} = 0$$

This leads to two complicated equations in integer powers of v_1 and v_2. Solving them in general is difficult. However, if we decide to look only for the solutions along $v_1 = v_2$, then both equations reduce to the same equation in k, the common value of v_1 and v_2. This shows that there is a solution along $v_1 = v_2$. The equation is:

$$\frac{32\pi^2 L^4}{l_p^2 d(d-1)}\left(1-\frac{1}{d(d-1)}\right)\frac{1}{k^2}-\frac{1}{4}(q^2+p^2)\frac{1}{k}=0$$

This gives

$$k=\frac{128\pi^2 L^4}{l_p^2 d(d-1)(q^2+p^2)}\left(1-\frac{1}{d(d-1)})\right)$$

Thus, an extremum of the entropy function is at:

$$v_1=v_2=\frac{128\pi^2 L^4}{l_p^2 d(d-1)(q^2+p^2)}\left(1-\frac{1}{d(d-1)}\right), e=\frac{q}{4\pi}$$

Now, we can find the extremal value of the entropy function:

$$\varepsilon_{ext}=\frac{16\pi^2 L^2}{l_p^2}\left(1-\frac{1}{d(d-1)}\right)^2+\frac{1}{4}(q^2+p^2)$$

Hence we have found the entropy of an extremal black hole with electric charge q and magnetic charge p, starting with a general higher derivative gravity coupled to Maxwell's action.

7. CONCLUSION

We calculated the entropy function for black holes in a general higher derivative gravity. We found that the entropy function and the scale factors of the factorised AdS and the 2-sphere geometries extremise to a constant that depends only on the electric and magnetic charges involved, the length scale in the cosmological constant, the Planck length and the dimensionality of the space-time.

References

[1] Robert M. Wald *General Relativity* University Of Chicago Press (1984)

[2] John Preskill, *Black Holes and Information: A Crisis in Quantum Physics* Caltech Theory Seminar (1994).

[3] Atish Dabholkar and Suresh Nampuri, *Lectures on Quantum Black Holes*, Lect. Notes Physics (2012).

[4] Ashoke Sen, *Black Hole Entropy Function and the Attractor Mechanism in Higher Derivative Gravity*, JHEP (2005).

[5] Ashoke Sen, *Black hole entropy function, attractors and precision counting of microstates*, General Relativity and Gravitation Vol. 40 (2008).

[6] George Ruppeiner, *On universality of the pure Lovelock gravity for the generalized Nariai and Bertotti-Robinson solutions* Rev. Mod. Phys. Vol. 67 (2012).

[7] Arpan Bhattacharya, Ling-Yan Hung, Kallol Sen and Aninda Sinha, *On c-theorems in Arbitrary Dimensions* Physical Review (2012).

.

Dependence of Fanaroff-Riley break of radio galaxies on luminosity and redshift

Kamlesh Rajpurohit [1] **and Ashok K. Singal**[2]
[1] M.Sc., Dept. physics, Jai Narain Vyas Univ. Jodhpur (RAJ), India. Email: phy.kamlesh@gmail.com
[2] A&A Division, Physical Research laboratory, Ahmedabad, India. Email: asingal@prl.res.in

Abstract. We investigate the dependence of the Fanaroff-Riley (FR) 1/2 dichotomy of radio galaxies on their luminosities and redshifts. Because of a very strong redshift-luminosity correlation (Malmquist bias) in a flux-limited sample, any redshift-dependent effect could appear as a luminosity related effect and vice versa. A question could then arise – do all the morphological differences seen in the two classes (FR1 and 2 types) of sources, usually attributed to the differences in their luminosities, could as well be primarily a redshift-dependent effect? A sharp break in luminosity, seen among the two classes, could after all reflect a sharp redshift-dependence due to a rather critical ambient density value at some cosmic epoch. A doubt on these lines does not seem to have been raised in past and things have never been examined with this particular aspect in mind. We want to ascertain the customary prevalent view in the literature that the systematic differences in the two broad morphology types of FR1 and 2 radio galaxies are indeed due to the differences in their luminosities, and not due to a change in redshift. Here we investigate the dependence of FR1/2 dichotomy of radio galaxies on luminosity and redshift by using the 3CR sample, where the FR1/2 dichotomy was first seen, supplemented by data from two additional samples (MRC and B3-VLA), which go about a factor of 5 or more deeper in flux-density than the original 3CR sample. This lets us compare sources with similar luminosities but at different redshifts as well as examine sources at similar redshifts but with different luminosities, thereby allowing us a successful separation of the otherwise two intricately entangled effects. We find that the morphology type is not directly related to redshift and the break between the two types of morphologies seems to depend only upon the radio luminosity.

1. INTRODUCTION

One of the robust correlations in observational astronomy is between the morphology type of radio galaxies and their radio luminosity. First pointed out by Fanaroff & Riley (1974) that there is a very sharp dependence of the morphology type of radio galaxies on their luminosity so that almost all radio galaxies below a luminosity $P_{178} = 2 \times 10^{25}$ W Hz^{-1} sr^{-1} (for Hubble constant $H_0 = 50\,\mathrm{km\ s^{-1}\ Mpc^{-1}}$), are edge-darkened (called type I) in their brightness distribution, while all radio galaxies above this luminosity limit are more or less edge-brightened (called type II). This correlation has withstood the test of time (Miley 1980; Antonucci 1993, 2012; Urry & Padovani 1995; Kembhavi & Narlikar 1999). However, because of a very strong redshift-luminosity correlation

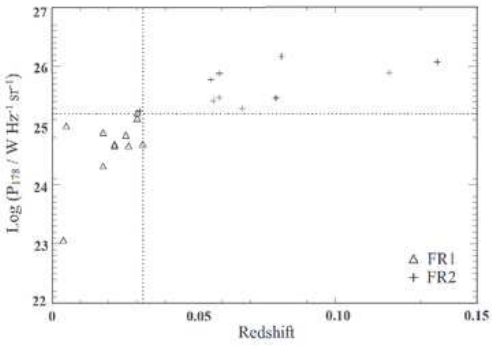

Figure 1. A scatter plot of both types of FR morphologies ('Δ' for edge-darkened FR I type and '$+$' for edge brightened FR II type) for the 3CR source sample of Fanaroff & Riley (1974) in the redshift-luminosity plane. To avoid undue compression of the scale, we have restricted the plot to a redshift limit of 0.15. There are no FR I type radio galaxies which lie beyond a redshift 0f 0.032 or have a luminosity $P_{178} > 2 \times 10^{25}$ W Hz^{-1} sr^{-1} (for $H_0 = 50\,\mathrm{km\ s^{-1}\ Mpc^{-1}}$) in the sample of Fanaroff & Riley.

(Malmquist bias) in a flux-limited sample, like in the 3CR sample used by Fanaroff & Riley (1974), any effect related with redshift could appear as a luminosity-dependent effect and vice versa. This then begs a question – could all the morphological differences seen in FR I and II types of sources be primarily due to a transition across some critical redshift value, manifesting a cosmological evolutionary effect due to a critical ambient density value at that redshift, instead of, as almost universally believed, an effect of transition across a certain critical luminosity value?

Following the archetypal paper by Fanaroff & Riley (1974), where they first pointed out the presence of two distinct morphology types of radio galaxies in the strong source 3CR sample, ascribing the distinct morphology of each galaxy to its radio luminosity, it has ever since been thought to be only a luminosity-dependent effect (see e.g., Saripalli 2012 and the references therein). There have been no attempts to investigate the alternative possibility that it could as well be a redshift-dependent effect, and thereby demonstrating the strong evolution of source morphology with cosmic epoch. For instance, suppose one wants to explore a correlation of the morphology type of radio galaxies with redshift. Figure 1 shows a scatter plot with redshift and luminosity of both types of morphologies classified by Fanaroff & Riley (1974) in their sample. The demarcation is as good with redshift as it is with luminosity. It might be a moot point to guess what would have been the verdict, had Fanaroff & Riley in their seminal paper tried a correlation against only redshift, instead of luminosity. It is quite likely the effect then would have been interpreted as due to a very strong cosmological evolution with redshift, and the subsequent theoretical interpretations in that case perhaps very different.

The two scenarios have very different physical interpretations, and either could be of equal importance. For instance in the conventional interpretation, with intrinsic luminosities being the root cause of their different morphology types, there is a huge amount of literature about the relation between the luminosity break and the different morphology types (Saripalli 2012 and the references therein). In fact all the models and discussions in the literature currently available are almost exclusively only within that framework. On the other hand a definite correlation with redshift alone would imply that it is the cosmic evolution of the properties of sources (perhaps because of the ambient density falling below a certain critical value due to the Hubble expansion) that might give rise to these two different type of morphologies, with FR I type being the current favourite and the FR II type "a thing of past".

All differences seen in FR I and FR II type sources, which are usually attributed to the differences in their luminosities, could as well be then related to the changing ambient densities with cosmic epoch. Also the very sharp division in luminosity could possibly be due to a critical ambient density value, which might divide the sources into two distinct morphology types. It might be the luminosity dependence or it might be the dependence on redshift that gives rise to these morphological differences, but this question could not be decisively settled based on any amount of arguments, sans actual observational data. At least this particular aspect has not yet been investigated in the literature. We may add that there are reports of FR I types seen at redshifts larger than $z > 0.5$ (Saripalli et al. 2012), but a systematic investigation of this question is still needed using samples which are complete in the sense that all FR I's above the sensitivity limit of the sample are included.

2. THE SAMPES AND THE DATA

One needs data from different samples to disentangle the luminosity and redshift correlation in order to study the dependences of FR I and FR II break separately on them. That is, to make these investigations one needs sufficient data comprising sources at different flux-density levels, so that one could examine sources with similar luminosities at different redshifts as well as compare them at similar redshifts for different luminosities, thereby separating the two effects. We investigate this dependence of FR dichotomy of radio galaxies on luminosity and redshift by taking data from three such different samples. And since the transition value of luminosity or/and redshift may not be as sharp (see e.g., Baum et al. 1995 and the references therein) as inferred from the data used by Fanaroff & Riley (1974), we investigate the two effects by determining the median values of luminosity and redshift for FRI type sources in every one of our selected samples.

Our first sample is the 3CR (Laing, Riley & Longair 1983), which is a complete strong source sample, with all necessary optical and radio information with good resolution maps so that one can in most cases unambiguously decide the FR I/II type of morphologies.

The second sample we have chosen is the essentially complete MRC (Molonglo Reference Catalog) sample (Kapahi et al. 1998) with $S_{408} \geq 0.95$ Jy, which is about a factor ~ 5 deeper than the 3CR sample and has the required radio and optical information. Their total sample comprises 550

sources, with 111 of them being quasars and the remainder radio galaxies. Optical identifications for the latter are complete up to a red magnitude of ~ 24 or a *K* magnitude of ~ 19 and among the still unidentified ones, which are expected to be at high redshifts $z \gtrsim 1$ and therefore of high luminosities as well, it is unlikely that there would be many FR I types.

For our third sample we have chosen a homogeneous sub-sample, known as B3-VLA, from B3 sources with $S_{408} > 0.1$ Jy, for which the relevant radio and optical information is given by Vigotti et al. (1989). Again the B3-VLA sample is expected to be complete at least as far as FR I type sources are concerned. Their VLA maps at 1415 MHz with 15 arcsec resolution are in general good enough for the morphologies to be classified into FR I/II types.

To quantitatively distinguish between FR I and II, following Fanaroff & Riley (1974), we classify a radio galaxy as FR I if the separation between the points of peak intensity in the two lobes is smaller than half the largest size of the source. Similarly FR II is the one in which the separation between the points of peak intensity in the two lobes is greater than half the largest size of the source. This is equivalent to having the "hot spots" nearer to (FR I) or further away from (FR II) the central optical galaxy than the regions of diffuse radio emission. In all the three samples we have examined the radio maps and using the above criteria, we have classified each source into either of the two types (FR I and II). There were a small number of sources that had a doubtful classification, we have dropped them from our analysis and that should not be too detrimental to our conclusions.

The luminosity of a source in our sample is calculated from its flux density S_{178} and the spectral index α ($S \propto \nu^{-\alpha}$) as

$$P_{178} = S_{178}\mathcal{D}^2(1+z)^{1+\alpha}, \tag{1}$$

where $\mathcal{D}$ is the comoving cosmological distance calculated from the cosmological redshift z of the source. In general it is not possible to express $\mathcal{D}$ in terms of z in a close-form analytical expression and one may have to evaluate it numerically. For example, in the flat universe models ($\Omega_m + \Omega_\Lambda = 1, \Omega_\Lambda \neq 0$), $\mathcal{D}$ is given by (see e.g., Weinberg 2008),

$$\mathcal{D} = \frac{c}{H_0}\int_1^{1+z} \frac{\mathrm{d}z}{\left(\Omega_\Lambda + \Omega_m z^3\right)^{1/2}}\ . \tag{2}$$

For a given Ω_Λ, $\mathcal{D}$ can be evaluated from Eq. (2) by a numerical integration. Here Ω_m is the matter energy density (including that of the dark matter) and Ω_Λ is the vacuum energy (dark energy!) density, both defined in terms of the critical energy density $\Omega_\mathrm{c} = 3H_0^2c^2/(8\pi G)$, where G is the gravitational constant and c is the velocity of light in vacuum. We have used $H_0 = 71\,\mathrm{km\ s^{-1}\,Mpc^{-1}}$, $\Omega_m = 0.27$ and $\Omega_\Lambda = 0.73$ (Spergel et al. 2003).

3. RESULTS AND DISCUSSIION

Figure 2 shows histograms of the distributions of radio galaxies with FR I type morphology against redshift for all our three samples. We have restricted our plots to $z = 0.25$ only, as no FR I type radio galaxy is seen beyond this redshift in any of the three samples. We have determined median value

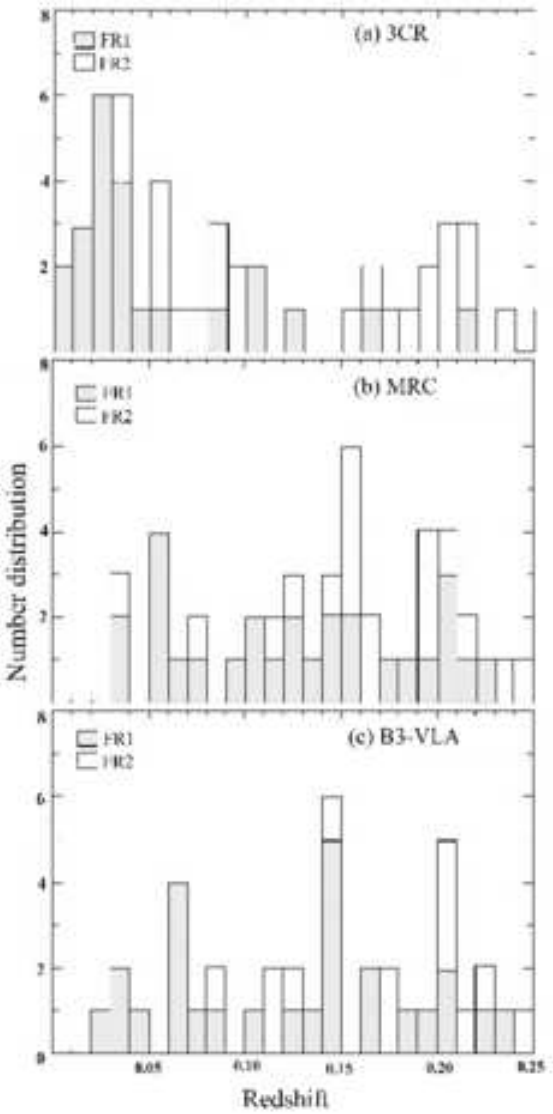

Figure 2. Histograms showing distributions of FR I/II morphology types radio galaxies with redshift for the (a) 3CR, (b) MRC and (c) B3-VLA samples. It should be noted that all radio galaxies seen beyond the redshift limit of the plots (i.e. $z > 0.25$) are only of FR II type in all of the above three samples.

z_{med} for the redshift distribution of FR I sources for each sample. The details of the method for determining the median values and for the estimation of their rms errors are described in Singal (1988). Figure 3 shows similar histograms of the distribution of radio galaxies with FR I type morphology against luminosity (at 178 MHz) for our three samples. Since all the FR I's we are interested in are at low redshifts ($z < 0.25$), the specific cosmological parameters do not make much difference for the luminosity evaluations except for the scaling factor due to the Hubble constant, which in our case makes luminosity estimates lower by a factor of $(71/50)^2 \approx 2$ than the calculations in Fanaroff & Riley (1974). Thus the FR I/II luminosity break of $P_{178} = 2 \times 10^{25}$ W Hz^{-1} sr^{-1} (for $H_0 = 50$ km s^{-1} Mpc^{-1}), arrived at by Fanaroff & Riley (1974) in their seminal paper, corresponds to $P_{178} = 10^{25}$ W Hz^{-1} sr^{-1} in our case. Again we have restricted our plots to $P_{178} = 10^{27}$ W Hz^{-1} sr^{-1} only, as no FR I type radio galaxy is seen beyond this luminosity value in any of the three samples.

From Figure 3, it is also clear that the FR I/II break is not as sharp as stated in Fanaroff & Riley (1974), as some overlap of both type of morphologies is seen in luminosity. However there is no denying that in all samples there are only a few, if any, FR I types with luminosities $P_{178} > 10^{26}$ W Hz^{-1} sr^{-1}.

Table 1. Percentile values of redshift and luminosity distributions for the FR I sources in the three samples.

Sample	$S_{178,\mathrm{med}}$	Number	z_{med}	z_{lq}	z_{uq}	$\log(P_{178,\mathrm{med}})$	$\log(P_{178,\mathrm{lq}})$	$\log(P_{178,\mathrm{uq}})$
	Jy	FR I						
3CR	19.4	23	0.03 ± 0.005	0.02	0.08	24.6 ± 0.2	24.2	25.5
MRC	2.7	27	0.12 ± 0.015	0.06	0.17	24.9 ± 0.1	24.6	25.2
B3-VLA	1.7	26	0.13 ± 0.015	0.06	0.16	24.7 ± 0.2	24.2	25.0

In Table 1 we have listed the median values both for the redshift and the luminosity in each of the three samples. Also listed are the median flux-density of FR I's in each sample and the number of FR I sources in the sample. The rms error in z_{med} in each case is determined from the frequency distribution (histogram) of z-distribution. The rms error is given by $\sqrt{n}/(2f_p)$ in units of the class interval of z (Kendall 1945; Yule & Kendall 1950), where n is the total number of sources in the sample and f_p is the ordinate value of the smoothed frequency distribution at the median value in Figure 2. The median value of the distribution does seem to shift substantially with redshift for samples which differ in flux-density by a factor of ~ 5 to 10. P_{med} and the rms error in P_{med} in each case is determined from the frequency distribution (histogram) of P-distribution in Figure 3, in the same way as for z_{med} as described above. Within errors there is hardly any difference in three samples in the P_{med} value, which thus seems to be independent of the flux-density level of the sample.

While the median value of redshift (z_{med}) differs for the weaker samples as much as a factor of about four, at about a 5σ level, as compared to that in the stronger 3CR sample, the difference

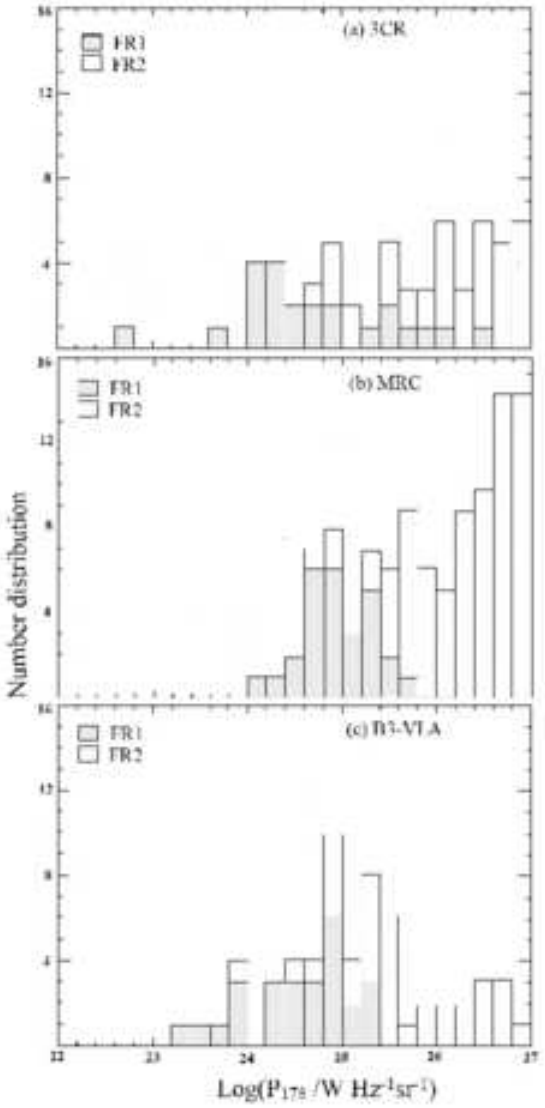

Figure 3. Histograms showing distributions of FR I/II morphology types radio galaxies with radio luminosity (P_{178} in units of W Hz^{-1} sr^{-1}) for the (a) 3CR, (b) MRC and (c) B3-VLA samples. It should be noted that all radio galaxies seen beyond the luminosity limit of the plots (i.e. $P_{178} > 10^{27}$ W Hz^{-1} sr^{-1}) are only of FR II type in all of the above three samples.

in the median value of luminosity ($P_{\rm med}$) is only marginal, being only a factor of about $10^{0.3} \sim 2$ and that too within only about 1σ. ¿From $z_{\rm med}$ and log($P_{\rm med}$) values, it is clear that the FR I type of morphology of radio galaxies is indeed due to their luminosity below a critical value as indeed envisaged first time by Fanaroff & Riley (1974) and that it is not directly related to the redshift and hence not due to a cosmic evolution effect.

To ascertain it further we have examined the normalized cumulative distributions of FR I morphology type radio galaxies with redshift as well as luminosity. Figure 4 shows the normalized cumulative distributions of FR I morphology type radio galaxies with redshift for the three samples. From this figure we can compare the relative numbers of FR I types upto any given redshift for different samples, and thereby for different radio luminosities. If the morphology type depended only on redshift and not on luminosity, then all the three normalized cumulative distributions in Figure 4 should be more or less coincident, which definitely is not the case.

In Table 1 we have listed, along with the median value ($z_{\rm med}$), also the lower quartile ($z_{\rm lq}$) and upper quartile ($z_{\rm uq}$) of the cumulative distribution of the redshifts of the sources in the three samples. We see that the space distribution of FR I morphology type radio galaxies does change with the

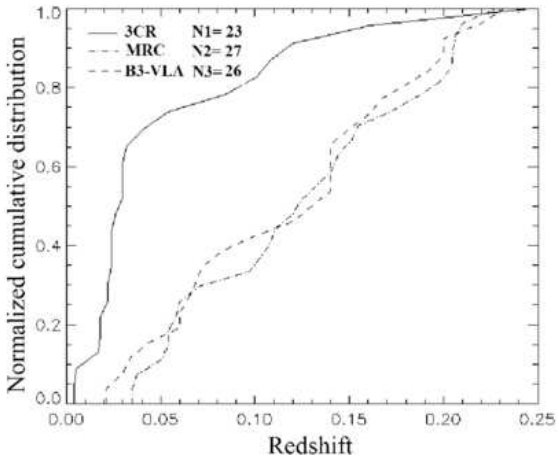

Figure 4. Normalized cumulative distributions of FR I morphology type radio galaxies with redshift for the (a) 3CR sample (continuous curve), (b) MRC sample (dot–dashed curves) and (c) B3-VLA sample (dashed curve). N1, N2 and N3 give the number of FR I radio galaxies in the 3CR, MRC and B3-VLA samples, respectively.

flux-density levels of the sample. There is a large difference in the redshift distribution of the 3CR sample from those of the MCR or B3-VLA samples, the latter two (MRC and B3-VLA samples) however, have statistically almost indistinguishable redshift distributions of the FR I radio galaxies, not surprising as they are at about similar flux-density levels, while the 3CR sample is about 5 to 10 times stronger in flux-density than the other two samples. It does seem that the redshift distribution

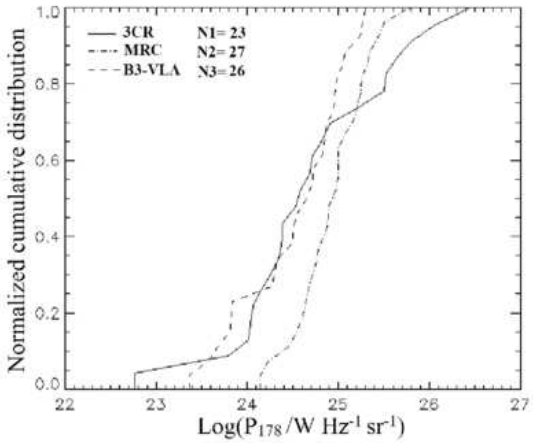

Figure 5. Normalized cumulative distributions of FR I morphology type radio galaxies with radio luminosity (P_{178} in units of W Hz^{-1} sr^{-1}) for the (a) 3CR sample (continuous curve), (b) MRC sample (dot–dashed curves) and (c) B3-VLA sample (dashed curve). N1, N2 and N3 give the number of FR I radio galaxies in the 3CR, MRC and B3-VLA samples, respectively.

of the FR I radio galaxies depends heavily on the flux-density level of the sample.

Figure 5 shows the normalized cumulative distribution of radio luminosity for FR I morphology type radio galaxies for our three samples. The three distributions overlap and there seems to be no gross difference in the luminosity distribution of FR I sources in the three samples. In Table 1 we have also listed the lower quartile ($P_{\rm lq}$) and upper quartile ($P_{\rm uq}$) of the cumulative distribution of the radio luminosity of the source in the three samples, which again are of very similar values for all three samples. From these we find that half of FR I types lie in the narrow range of luminosities $P_{178} \sim 10^{24.7\pm0.5}$ W Hz^{-1} sr^{-1}, that is within a factor of 3 around 5×10^{24} W Hz^{-1} sr^{-1}. Also all galaxies with radio luminosity above $P_{178} \sim 10^{26.5}$ W Hz^{-1} sr^{-1} are only of type II with an edge brightened morphology. We have thus reaffirmed that the FR I/II dichotomy is due to a change in luminosity below and above a certain critical level, as first proposed by Fanaroff & Riley (1974) and followed in the literature ever since, and that it is not due to any cosmic epoch dependent evolution that gives rise to different FR I and II type morphologies.

4. CONCLUSIONS

We have investigated if there is a direct dependence of the FR I and II morphology types of the radio galaxies on redshift. For this we compared their distributions in three different samples with different flux-density limits, which allowed us to separately study the effects of redshift and/or radio luminosity on the occurrences of the two morphology types. It was shown that the morphology

type is not directly related to redshift and thereby not a cosmic epoch dependent effect. The break between the two types of morphologies seems to depend only upon the radio luminosity. Half of the FR I type radio galaxies lie in the narrow range of luminosities $P_{178} \sim 10^{24.7\pm0.5}$ W Hz^{-1} sr^{-1}, with none exceeding the value $P_{178} \sim 10^{26.5}$ W Hz^{-1} sr^{-1}, above which all were found to be exclusively type II with an edge brightened morphology.

ACKNOWLEDGEMENTS

KR expresses her gratitude to the Astronomy and Astrophysics Division of the Physical Research laboratory Ahmedabad, where work on this summer project was done under the guidance of AKS.

References

[1] Antonucci, R. 1993, ARAA, 31, 473
[2] Baum, A. A., Zirbel, E. L., O'Dea, P. 1995, ApJ, 451, 88
[3] Fanaroff B. L., Riley J. M. 1974, MNRAS, 167, 31P
[4] Kapahi, V. K., Athreya, R. M., van Breugel, W., McCarthy, P. J., Subrahmanya, C. R. 1998, ApJS, 118, 275.
[5] Kembhavi, A. K., Narlikar, J. V. 1999, Quasars and Active Galactic Nuclei – An Introduction (Cambridge: Camb. Univ.), 357
[6] Kendall, M. G. 1945, The Advanced Theory of Statistics, vol. 1 (London: Charles Griffin), 211
[7] Laing R. A., Riley J. M., Longair M. S. 1983, MNRAS, 204, 151
[8] Miley, G. K. 1980, ARAA, 18, 165
[9] Saripalli, L. 2012, AJ, 144, 85
[10] Saripalli, L., Subrahmanyan, R., Thorat, K. et al. 2012, ApJS, 199, 27
[11] Singal A. K. 1988, MNRAS, 233, 87
[12] Spergel, D. N., Verde, L., Peiris, H. V. et al. 2003, ApJS, 148, 175
[13] Urry, C. M., Padovani, P. 1995, PASP, 107, 803
[14] Vigotti M., Grueff G., Perley R., Clark B. G., Bridle A. H. 1989, AJ, 98, 419
[15] Weinberg, S. 2008, Cosmology (Oxford: Oxford Univ.), 43
[16] Yule, U. G., Kendall, M. G. 1950, An Introduction to the Theory of Statistics (London: Charles Griffin), 425

Averaging Theory for Weakly Nonlinear Oscillators*

Aritra Sinha
Department of Physics and Astronomy,National Institute of Technology Rourkela Address: Sector - 2 Rourkela, Odisha-769008

Abstract. In this short paper, I have first discussed how averaging theory can be an effective tool in solving weakly non-linear oscillators. Then I have applied this technique for a Van der Pol oscillator and extended the stability criterion of a Van der Pol oscillator for any integer n(odd or even).

1. WEAKLY NONLINEAR OSCILLATORS

We consider systems of the form

$$\ddot{\mathbf{x}} + \mathbf{x} + \epsilon \mathbf{h}(\mathbf{x}, \dot{\mathbf{x}}) = \mathbf{0}$$

where $0 \leq \epsilon \ll 1$ and $h(x, \dot{x})$ is an arbitrary smooth function.

Since such equations represent small perturbations of the linear oscillator $\ddot{x} + x = 0$, they are called **weakly nonlinear oscillators**.

Some well known examples are the **Van der Pol** equation

$$\ddot{x} + x + \epsilon(x^2 - 1)\dot{x} = 0$$

and the **Duffing** equation

$$\ddot{x} + x + \epsilon x^3 = 0.$$

For the Van der Pol equation in $(\mathbf{x}, \dot{\mathbf{x}})$ phase space, if we choose an initial condition close to the origin and ϵ near 0, the trajectory is a slowly winding spiral; it takes many cycles for the amplitude to grow substantially. Eventually the trajectory asymptotes to an approximately circular limit cycle whose radius is close to 2. There are various ways one can exploit the fact, that oscillator is **close** to a simple harmonic oscillator, to produce useful approximations. Here I will use the method of averaging theory to predict the period and radius of the limit cycle.

2. AVERAGING THEORY

2.1 *Introduction*

Our system is

$$\ddot{x} + x + \epsilon h(x, \dot{x}) = 0$$

*aritrasinha98@gmail.com

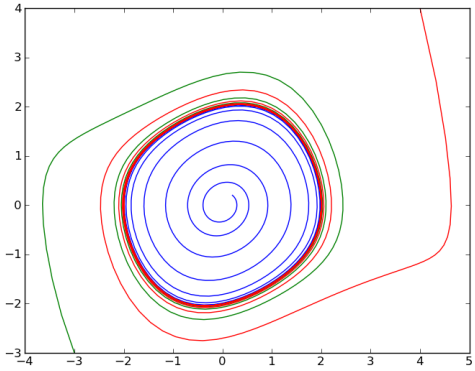

Figure 1.

where

$$0 \leq \epsilon \ll 1$$

Let

$$\dot{x} = y \;\; \dot{y} = -x - \epsilon h(x, y)$$

When $\epsilon = 0$, the solutions are

$$x(t) = r\cos(t + \phi)$$

$$y(t) = -r\sin(t + \phi)$$

where r,ϕ are **constant** for simple harmonic oscillator on trajectories.

When $\epsilon \neq 0$, we expect a very slow drift of r and ϕ. They would evolve as expected; might approach a limit cycle. Our task at hand is to find the evolution equations of the amplitude and the phase given the effect of this nonlinear term $h(x, y)$. We can be definite that since ϵ is extremely small, the trajectories would be nearly circular and they would have periods of 2π approximately.

Now let

$$x(t) = r(t)\cos(t + \phi(t))$$

$$y(t) = -r(t)\sin(t + \phi(t))$$

Note here that although it might seem that the calculus done is wrong in computing y, but it is not so. Instead let it be a definition.

So view this as definition of $r(t)$ and $\phi(t)$ i.e.

$$r(t) = \sqrt{x^2(t) + y^2(t)}$$

$$\tan\left(t + \phi(t)\right) = -\frac{y(t)}{x(t)}$$

2.2 *Calculating $\dot{r}$ and $\dot{\phi}$*

Let us find equations for $\dot{r}$, $\dot{\phi}$:

$$\begin{aligned}
r^2 &= x^2 + y^2 \\
\implies r\dot{r} &= x\dot{x} + y\dot{y} \\
&= x(y) + y(-x - \epsilon h) \\
&= -\epsilon y h \\
&= -\epsilon h(-r\sin\left(t + \phi\right)) \\
\implies \dot{r} &= \epsilon h \sin\left(t + \phi\right)
\end{aligned}$$

$$\begin{aligned}
\frac{d}{dt}(t + \phi(t)) &= \tfrac{d}{dt}\left(\arctan - \tfrac{y(t)}{x(t)}\right) \\
\implies 1 + \dot{\phi}(t) &= \left(\tfrac{1}{1+\frac{y^2}{x^2}}\right)\tfrac{d\left(-\frac{y}{x}\right)}{dt} \\
&= \tfrac{x^2}{x^2+y^2}\left[-\left(\tfrac{1}{x}\dot{y} - \tfrac{y}{x^2}\dot{x}\right)\right] \\
&= \tfrac{x^2}{x^2+y^2}\left[\tfrac{y}{x^2}\dot{x} - \tfrac{\dot{y}}{x}\right] \\
&= \tfrac{1}{x^2+y^2}\left[y\dot{x} - x\dot{y}\right] \\
&= \tfrac{1}{x^2+y^2}\left[y^2 + x^2 + \epsilon x h\right] \\
1 + \dot{\phi} &= 1 + \tfrac{\epsilon h x}{x^2+y^2}
\end{aligned}$$

Now since

$$x^2 + y^2 = r^2 \ \text{ and } \ x = r\cos\left(t + \phi(t)\right)$$

we have,

$$\boxed{\dot{\phi} = \frac{\epsilon h}{r}\cos\left(t + \phi\right)}$$

So we get slowly varying amplitude and phase, as expected, of the order ϵ.

$$\dot{r} = \mathrm{O}(\epsilon), \dot{\phi} = \mathrm{O}(\epsilon)$$

3. MAIAN CONCEPT OF AVERAGING

Now what we have to do is exploit the separation of time scales of the evolution equations - **fast oscillation** versus **slow drift**. The main idea is to iron out the fast oscillations by averaging over one cycle of length 2π (1 oscillation) so that we can find out the explicit dependence of the evolution equations on ϵ.

A **practical example** of the averaging theory would be our primary detector, eyes. All the things we see around us are made up of rapidly vibrating atoms. But our detectors average out this fast oscillation and we see only the slow scale dynamics explicitly.

Given $g(t)$,let us define the average over one cycle about the point t as

$$< g > (t) = \frac{1}{2\pi} \int_{t-\pi}^{t+\pi} g(s)\, ds.$$

So let us write out the equations for $\bar{r}$ and $\bar{\phi}$.

$$\dot{\bar{r}} =< \epsilon h \sin(t+\phi) >_t$$

$$\dot{\bar{\phi}} = \langle \frac{\epsilon h}{r} \cos(t+\phi) \rangle_t$$

These equations are exact since $R.H.S.$ depends on r,ϕ, not $\bar{r}$, $\bar{\phi}$.

Now here you will notice a subtle difficulty, since we want a dynamical system with $\bar{r}$ and $\bar{\phi}$ so that we can compute the averages. We can get over this problem with an approximation. We well know that there is only a slight difference between r and $\bar{r}$. [It is comparable to our height measured right at this instant versus our height averaged over the past. That is sort of the same thing with a slight error.] It is here that we are going to introduce an approximation.

Over one cycle,

$$r = \bar{r} + \mathrm{O}(\epsilon)\phi = \bar{\phi} + \mathrm{O}(\epsilon)$$

Now we will replace r,ϕ by $\bar{r}$,$\bar{\phi}$ in the evolution equations which causes $\mathrm{O}(\epsilon^2)$ in the **ODE'S**. The beauty of this is that we get autonomous equations which we can analyse easily with phase plane methods. So the formal evolution equations are

$$\dot{\bar{r}} =< \epsilon h \sin(t+\phi) > +\mathrm{O}(\epsilon^2) \dot{\bar{\phi}} = \left\langle \tfrac{\epsilon h}{r} \cos(t+\phi) \right\rangle + \mathrm{O}(\epsilon^2)$$

We should treat $\bar{r}$ and $\bar{\phi}$ as constants while performing the averages.

4. APPLICATOIN ON GENERA VAN DER POL OSCILLATOR

Now we shall apply this averaging technique to a general case of Van der Pol's oscillator. The general Van der Pol equation is-

$$\ddot{x} + x + \epsilon \dot{x}(x^n - 1) = 0, \;\; 0 \leq \epsilon \ll 1 \;\; n \;\; \epsilon \;\; \mathbf{N}$$

I will try to show that when n is odd, r is going to grow exponentially and when n is even, r approaches a limit cycle.

I am going to use "$<\ >$" symbols which essentially means average over one cycle. We need to remember from previous discussions that $x = r\cos(t+\phi)$,$y = -r\sin(t+\phi)$ and $\dot{x} = y$. Let $(t+\bar{\phi})$ be replaced by θ in the following math.

$$h(x,\dot{x}) = (x^n - 1)\dot{x} = (x^n - 1)y$$

$$= (\bar{r}^n \cos^n(t+\bar{\phi}) - 1)(-\bar{r}\sin(t+\bar{\phi})) + \mathrm{O}(\epsilon)$$

$$= -\bar{r}^{n+1}\cos^n\theta\sin\theta + \bar{r}\sin\theta + \mathrm{O}(\epsilon)$$

$$\dot{\bar{r}} =< \epsilon h\sin\theta > +\mathrm{O}(\epsilon^2)$$

$$= \left\langle \epsilon(\bar{r}\sin\theta - \bar{r}^{n+1}\cos^n\theta\sin\theta)\sin\theta \right\rangle + \mathrm{O}(\epsilon^2)$$

$$= \epsilon\bar{r}\left\langle \sin^2\theta \right\rangle - \epsilon\bar{r}^{n+1}\left\langle \cos^n\theta\sin^2\theta \right\rangle + \mathrm{O}(\epsilon^2)$$

$$= \frac{\epsilon\bar{r}}{2} - \epsilon\bar{r}^{n+1}\left\langle \cos^n\theta\sin^2\theta \right\rangle + \mathrm{O}(\epsilon^2)$$

$$\dot{\bar{\phi}} = \left\langle \frac{\epsilon h}{r}\cos(t+\phi) \right\rangle + \mathrm{O}(\epsilon^2)$$

$$= \left\langle \frac{\epsilon}{\bar{r}}(-\bar{r}^{n+1}\cos^n\theta\sin\theta + \bar{r}\sin\theta)\cos\theta \right\rangle + \mathrm{O}(\epsilon^2)$$

$$= \left\langle \epsilon(-\bar{r}^n\cos^{n+1}\theta\sin\theta + \sin\theta\cos\theta) \right\rangle + \mathrm{O}(\epsilon^2)$$

$$= -\epsilon\bar{r}^n\left\langle \cos^{n+1}\theta\sin\theta \right\rangle + \epsilon\left\langle \sin\theta\cos\theta \right\rangle + \mathrm{O}(\epsilon^2)$$

$$= \mathrm{O}(\epsilon^2)[\because\ both\ \ \left\langle \cos^{n+1}\theta\sin\theta \right\rangle\ \ and\ \ \left\langle \sin\theta\cos\theta \right\rangle\ \ are\ \ equal\ \ to\ \ 0.]$$

4.1 *When n is Odd*

Let $n = 2m+1$.

$$\left\langle \cos^{2m+1}\theta\sin^2\theta \right\rangle$$

$$= \int_0^{2\pi} \cos^{2m+1}\theta\sin^2\theta\, d\theta$$

[Now let $t = \sin\theta$, then $dt = \cos\theta d\theta$]

$$= \int_0^0 (1-t^2)^{2m}t^2\, dt = 0.$$

So for odd n,

$$\dot{\bar{r}} = \frac{\epsilon\bar{r}}{2} + \mathrm{O}(\epsilon^2)$$

If we neglect $\mathrm{O}(\epsilon^2)$ error, then

$$\frac{d\bar{r}}{dt} = \frac{\epsilon\bar{r}}{2}$$

$$\implies \frac{d\bar{r}}{\bar{r}} = \frac{\epsilon}{2}dt$$

$$\implies \log\bar{r} = \frac{\epsilon}{2}t + k \qquad [where \quad k \quad is \quad any \quad constant]$$

$$\therefore \bar{r} = \rho\exp\left(\frac{\epsilon}{2}t\right) \quad [where \quad \rho \quad is \quad a \quad constant \quad of \quad integration].$$

So the final approximate solution for odd n is

$$x = \rho\exp\left(\frac{\epsilon}{2}t\right)\cos(t+\phi).$$

Therefore we assert that x is going to blow up given sufficiently long time and the phase is going to change negligibly.

4.2 *When n is Even*

We can be sure, that since $\cos^n\theta\sin^2\theta$ is ≥ 0 throughout, $\left\langle\cos^n\theta\sin^2\theta\right\rangle$ must be equal to some positive quantity say k^2.

$$\dot{\bar{r}} = \frac{\epsilon\bar{r}}{2} - \epsilon\bar{r}^{n+1}k^2$$

$$= \frac{\epsilon\bar{r}}{2}(1 - 2\bar{r}^n k^2)$$

So $\bar{r}$ has one real positive root $\left(\frac{1}{2k^2}\right)^{\frac{1}{n}}$. Whenever $\bar{r}$ is greater than $\left(\frac{1}{2k^2}\right)^{\frac{1}{n}}$, $\dot{\bar{r}}$ is less than 0 and $\bar{r}$ continues to shrink till it reaches $\left(\frac{1}{2k^2}\right)^{\frac{1}{n}}$. And whenever $\bar{r}$ is less than $\left(\frac{1}{2k^2}\right)^{\frac{1}{n}}$, $\dot{\bar{r}}$ is greater than 0 and $\bar{r}$ continues to grow till it reaches $\left(\frac{1}{2k^2}\right)^{\frac{1}{n}}$. So this means that the oscillator is going to approach a limit cycle of amplitude 2. This is the beauty of the problem when n is even. Now let's do a problem based on this.

Example: Let us consider a Van der Pol oscillator

$$\ddot{x} + x + \epsilon\dot{x}(x^2 - 1) = 0, \qquad 0 \leq \epsilon \ll 1$$

$$h(x,\dot{x}) = (x^2-1)\dot{x} = (x^2-1)y$$

$$= (\bar{r}^2\cos^2(t+\bar{\phi}) - 1)(-\bar{r}\sin(t+\bar{\phi})) + \mathrm{O}(\epsilon)$$

$$\dot{\bar{r}} =< \epsilon h\sin(t+\phi) > + \mathrm{O}(\epsilon^2)$$

$$= \left\langle\epsilon(\bar{r}\sin\theta - \bar{r}^3\cos^n\theta\sin\theta)\sin\theta\right\rangle + \mathrm{O}(\epsilon^2)$$

$$= \epsilon\bar{r}\left\langle\sin^2\theta\right\rangle - \epsilon\bar{r}^3\left\langle\cos^n\theta\sin^2\theta\right\rangle + \mathrm{O}(\epsilon^2)$$

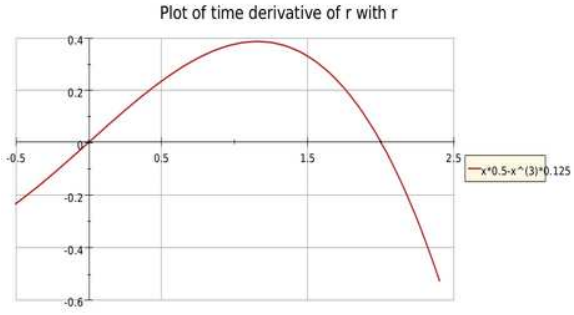

Figure 2.

$$= \frac{\epsilon \bar{r}}{2} - \frac{\epsilon \bar{r}^3}{8} + \mathrm{O}(\epsilon^2)$$
$$= \frac{\epsilon \bar{r}}{8}(4 - \bar{r}^2) + \mathrm{O}(\epsilon^2)$$

From the diagram it is clear that as t tends to ∞, value of $\bar{r}$ tends to 2. It means that after sufficiently long time,the Van der Pol Oscillator settles down to a limit cycle of amplitude 2.
$\dot{\bar{\phi}} \sim \mathrm{O}(\epsilon^2)$ [proved earlier in the general case] So ϕ changes on super slow time-scale. Period of the Van der Pol oscillator $= 2\pi + \mathrm{O}(\epsilon^2)$.

References

[1] Nonlinear Dynamics and Chaos [With Applications to Physics, Biology, Chemistry and Engineering],*Levant Books*, **Steven H. Strogatz**

[2] Video lecture titled *MAE5790-11 Averaging theory for weakly nonlinear oscillators* by the YouTube Channel **Cornell MAE** given by **Prof. Steven Strogatz**

.

STUDENT JOURNAL OF PHYSICS
IAPT

Volume 5 **Number 4** **June 2016**

CONTENTS